ELECTROSTATIC MICROACTUATOR CONTROL SYSTEM FOR FORCE SPECTROSCOPY

A Thesis
Presented to
The Academic Faculty

by

Ofer Finkler

In Partial Fulfillment
of the Requirements for the Degree
Masters of Science in the
School of Electrical and Computer Engineering

Georgia Institute of Technology
November 2009

ELECTROSTATIC MICROACTUATOR CONTROL SYSTEM FOR FORCE SPECTROSCOPY

Approved by:

Professor F Levent Degertekin, Advisor
School of Mechanical Engineering
Georgia Institute of Technology

Professor Albert B Frazier
School of Electrical and Computer Engineering
Georgia Institute of Technology

Professor Oliver Brand
School of Electrical and Computer Engineering
Georgia Institute of Technology

Date Approved: 12 November 2009

To my parents,

Vitold & Rika Finkler,

ACKNOWLEDGEMENTS

I owe many thanks to all who made this thesis possible. I would first like to express my deep gratitude to my thesis advisor, Professor Levent Degertekin for his patience, motivation, enthusiasm, and immense knowledge. His guidance helped me throughout my research and writing of this thesis.

Professor Albert B Frazier and Professor Oliver Brand deserve a special thanks for serving as my thesis committee members, and for their guidance and support throughout my undergraduate as well as my graduate journey at the Georgia Institute of Technology. I doubt that I will ever be able to convey my appreciation fully for all of their help, but I owe them my eternal gratitude.

I am also grateful to all MiST group colleagues and especially to Hamdi Torun for all of his kind help, friendly support and enjoyable discussions.

Special thanks goes to Dr. Kong Fang from the Bioengineering Department for his time and support towards my research.

Lastly, I would like to thank my parents and sister for their love, support, and everything.

TABLE OF CONTENTS

LIST OF TABLES

LIST OF FIGURES

SUMMARY

Single molecule force spectroscopy is an important technique to determine the interaction forces between biomolecules. Atomic force microscopy (AFM) is one of the tools used for this purpose. So far, AFMs usually use cantilevers as the force sensors and piezoelectrics as the actuators which may have some drawbacks in terms of speed and noise.

In this research, a micromachined membrane actuator was used in two important types of experiments, namely the single molecule pulling and force-clamp based force spectroscopy. These two methods permit a more direct way of probing the forces of biomolecules, giving a detailed insight into binding potentials, and allowing the detection of discrete unbinding forces. To improve the quality of the experiments there is a need for high force resolution, high time resolution and increase in the throughput.

This research focuses on using the combination of AFM and membrane based probe structures that have electrostatic actuation capability. The membrane actuators are characterized for range, dynamics, and noise to illustrate their adequacy for these experiments and to show that the complexity they introduce does not affect the noise level in the system.

The control system described in this thesis utilizes the novel membrane actuator structures and integrates it into the current AFM setup. This is a very useful tool which can be implemented on any AFM without changing its mechanical architecture. To perform an experiment, all that is needed is to place the membrane actuator on the AFM stage, under the imagining head, and run the control system, which was implemented using LabVIEW.

The system allows the user to maintain a precise and continuous control of the force. This was demonstrated by performing a life time experiment using biomolecules. Moreover, by slightly modifying the control scheme, the system allows us to linearize the membrane motion, which is inherently non-linear. The feasibility of using this control system for a variety of loading rate experiments are also demonstrated.

CHAPTER I

INTRODUCTION

Binding force is an important functional and structural parameter in many biomolecules. This force is the result of weak noncovalent interactions which control different functions in cells. Because these are weak bonds, they are likely to unbind if pulled under any force for almost any period of time. When pulled at different speeds the bond will resist the detachment by a range of forces [7]. In order to understand the bond strength there is a need to understand the relation between force, lifetime, and chemistry at the molecular level.

Force spectroscopy has been developed to allow better understanding of this relation by having a closer look into the chemical energy landscape of the bond [8]. External steady ramp forces over a period of time lower the boundaries in the energy landscape. Therefore the unbinding forces depend on the loading rates, also refereed to as the slope of the force as a function of time. When performing the experiments the results might contain systematic errors as a result of multiple bonds to the substrate, and probe mechanics [9]. Therefore, in order to have statistically significant data, large number of measurements at each loading rate are obtained and only the most probable loading rate and force are used. Figure 1 illustrates how these values are chosen.

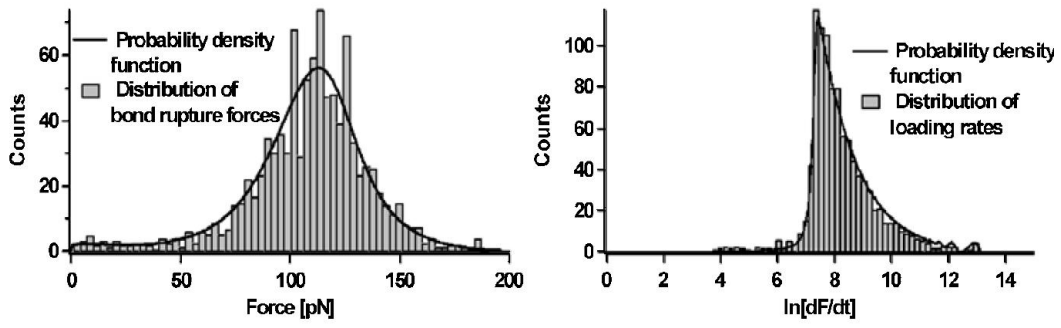

Figure 1: Histograms fitted by Gaussian curves in order to find the probable loading rate and force for further analysis [9].

The data collected is plotted in the form of histograms, which are usually fitted using a Gaussian curve. The values obtained from this plot are then used for the

loading rate analysis. Figure 2 shows a plot of different loading rates plotted against the corresponding most frequent rupture forces, obtained from the statistical analysis shown in Figure 1.

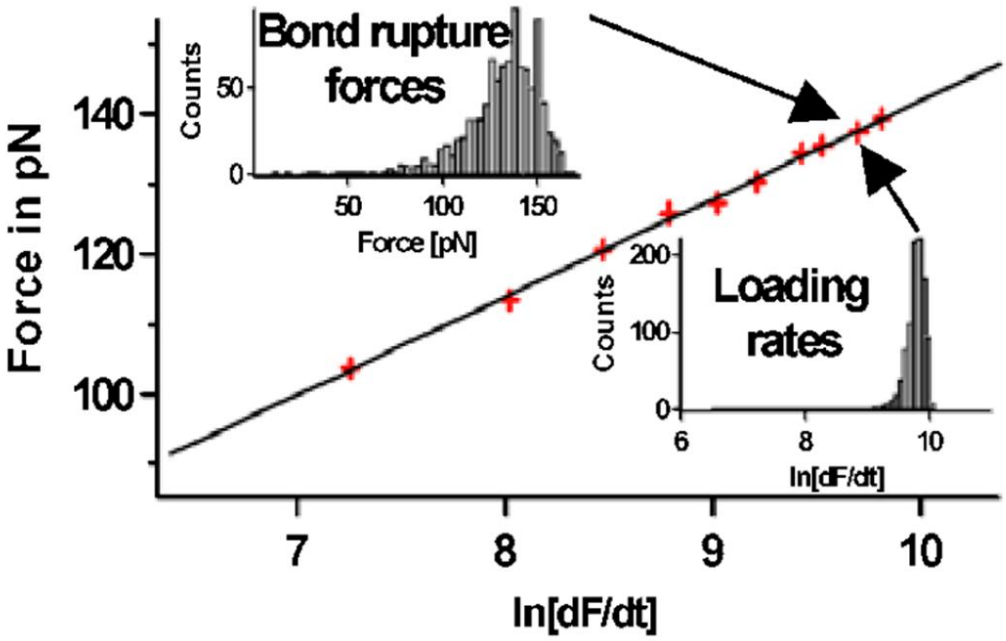

Figure 2: Linearization for the most probable rupture forces and their loading rates [9].

The results are plotted on a scale of log for the different loading rates. It was shown that there is a linear dependence of the force with respect to the log of the loading rate [9], and therefore a straight line will best fit the resulting data pairs. This shows that for lower loading rate the corresponding rupture force, which also decreases, will require the use of high force resolution detection systems. On the other hand, higher loading rates will require the system to have fast actuation capabilities. Using this analysis a dynamic spectrum can be established for the bond strength which images the prominent energy barriers traversed along the force-driven pathway.

The force dependency cannot be quantified by loading rate experiments only, and it is desirable to also perform these experiments under force-clamp conditions, which will allow a direct measurement of the unbinding and unfolding probability

dependency on the force. Again, as in the case of the loading rate experiments, only the most probable lifetimes will be considered for each force value. Figure 3 shows an example for the analysis obtained from this data.

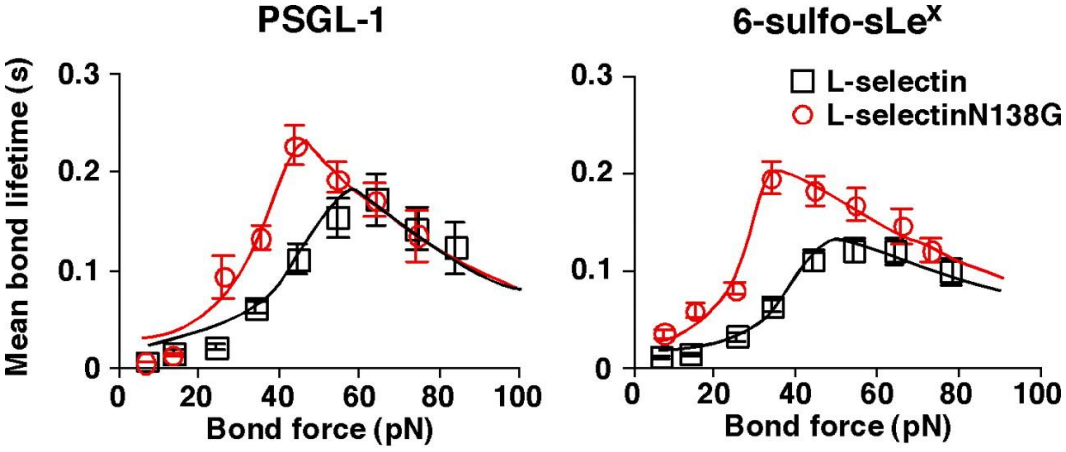

Figure 3: Lifetimes as a function of force for interactions of L-selectin and L-selectinN138G with PSGL-1 and 6-sulfo-sLe^x [21].

The plot shows the lifetime dependance on force for the interactions of L-selectin and L-selectinN138G with PSGL-1 and 6-sulfo-sLe^x [21]. It is very important to keep the system at force clamped conditions at all time. Therefore, a feedback system is needed to accommodate for any discrepancies in the force value. Again as in the case of the loading rate measurement, when using high force values the experiments will be done in the microsecond scale [1], and will require a fast feedback system. On the other hand, if lower forces will be used the experiment will be in the minute scale [34], which will require high stability.

Contributions of these experiments include the exploration of the energy landscapes of carbohydrate-(selectin)protein bonds [10], cooperative unbinding of short DNA duplexes [36], homotypic bonds between cadherins [3], unfolding of Ig domains in the muscle protein titin [28] and in recombinant proteins [22], and biotin-(strept)avidin bonds [23]. The last two applications mentioned will be demonstrated in this thesis.

Several techniques used for these experiment include the biomembrane force probe (BFP) [32], optical tweezers [2] magnetic beads [33], glass microneedles [18], and the atomic force microscopy (AFM) [24, 40] which is discussed in this thesis.

As mentioned before, the AFM system is addressed in this thesis. Most of the AFMs use a laser beam deflection systems. The laser is reflected from the back of the reflective AFM cantilever and onto a photodiode which acts as a position-sensitive sensor. Figure 4 illustrates this system.

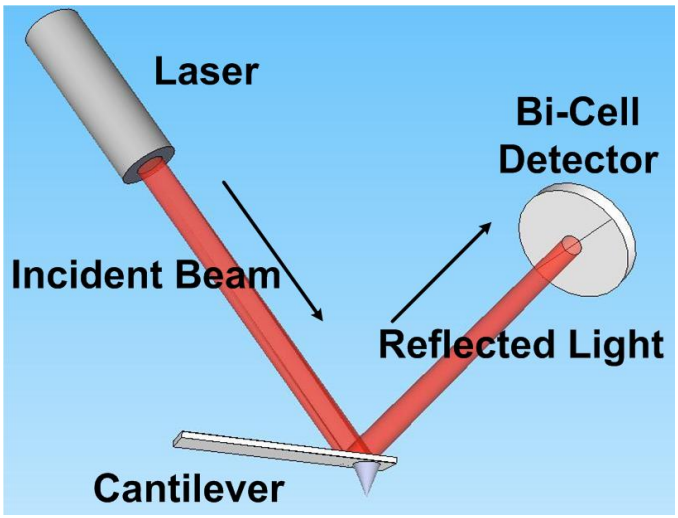

Figure 4: Illustration of the laser beam deflection system.

The AFM does not measure the forces between the tip and the sample directly. Instead, using Hook's law given in Equation 1, the force is calculated by measuring the deflection of the cantilever and multiplying it by the already known stiffness.

$$F = -kZ \tag{1}$$

This value is usually specified by the cantilever manufacturer or measured using a variety of methods [20].

The AFM has a number of applications which include contact mode, lateral force microscopy, noncontact mode, tapping mode, force modulation, and phase imaging.

The actuation capabilities of the AFM system are obtained through the use of a piezoelectric actuator tube. Commercial piezo actuators tubes have a frequency bandwidth of up to approximately 10 kHz [26], which might be problematic for different experiments which require faster operation [35]. Other issues with the AFM arise due to the cantilever probe limitation. The cantilever introduces issues such as the hydrodynamic drag effect in fluid experiments [29], which limit the frequency response of the cantilever and lowers the actuation bandwidth, and thermal drift [37] which creates stability problems. To avoid some of these issues, this thesis will discuss the use of an AFM system for force detection purposes only, while the actuation will be done using an electrostatic membrane actuator structure. Figure 5 shows an illustration that demonstrates how the system will be set up with a membrane actuator.

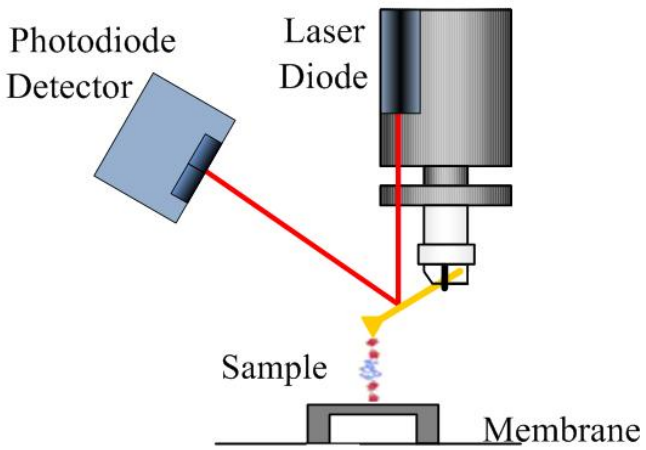

Figure 5: AFM system used with electrostatic membrane actuator structure.

This will enable the use of a broader range of actuation frequencies, but will still be limited by the frequency response of the AFM cantilever, which is used in these experiments for detection purposes. According to the cantilever manufacturer (MLCT-C cantilever, Veeco), the cantilever has a frequency response of 7 kHz. This value decreases drastically when used in fluid due to the hydrodynamic drag which was mentioned earlier. This drag is affected by the size of the cantilever used, where

larger cantilevers will create larger drag. Further description of the specific cantilever used in the experiments in this thesis will be given in chapter 3.

Using the AFM system, the pulling experiment is preformed by stretching the molecule from the tip of the cantilever, by a piezo drive, while measuring the force on the cantilever. Figure 6 shows a record of a typical force-distance cycle caused by the effect of antibody-antigen binding [14].

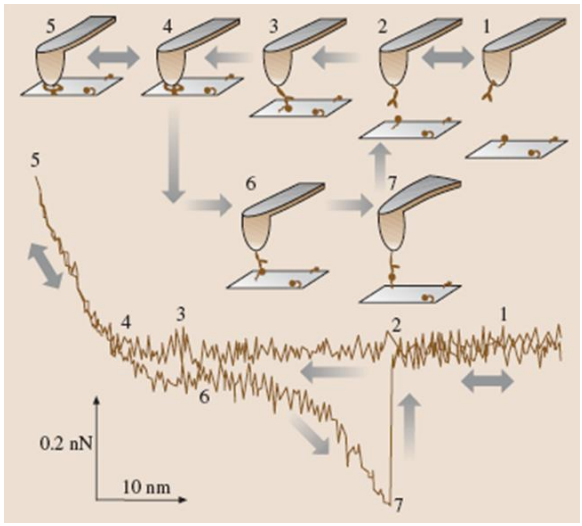

Figure 6: Detection of single antigen recognition events by a tip-antibody sensor [14].

The antibody is brought in contact with the antigen during which binding will occur. The binding causes an extra force signal during tip retraction, reflecting extension of the flexible connection until rupture occurs. As seen in Figure 6, and as mentioned earlier, it is very important to have high resolution in order to detect smaller forces. These forces are usually the result of slower loading rates. In molecule stretching experiments, the AFM cantilever is used for the extension of molecules such as the titin molecule to allow a closer look into the different molecule domains. Because the force applies on the molecule changes constantly, a complex time series of unfolding events is created resulting in a sawtooth pattern shown in Figure 7.

It is seen from the figure that the actuator has to have enough displacement to

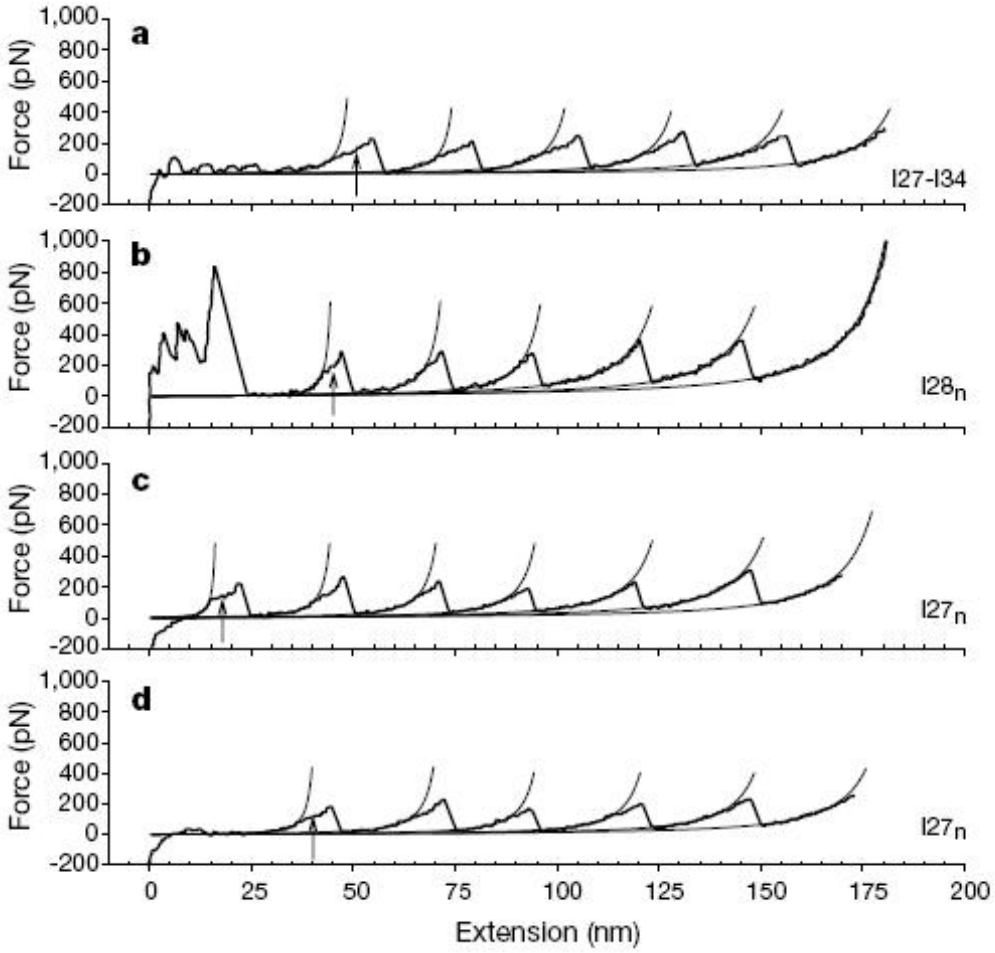

Figure 7: Measurements of a single partly unfolded titin protein [22]

accommodate for full extension of the molecule. Depending on the type of molecule used, this displacement can reach the length of approximately 400 nm [8].

In the force clamp experiments, done using the AFM system, the molecule is stretched by a predetermined constant force. Figure 8 shows an experiment preformed using a constant stretching force of 120 pN [30].

The force clamp experiments designed for these studies have proven problematic due to different reasons such as drift and mechanical vibrations. Some solutions were proven to eliminate the thermal drift [37, 41, 4], which is a significant source of drift, but the system still encountered fluctuations in the force value.

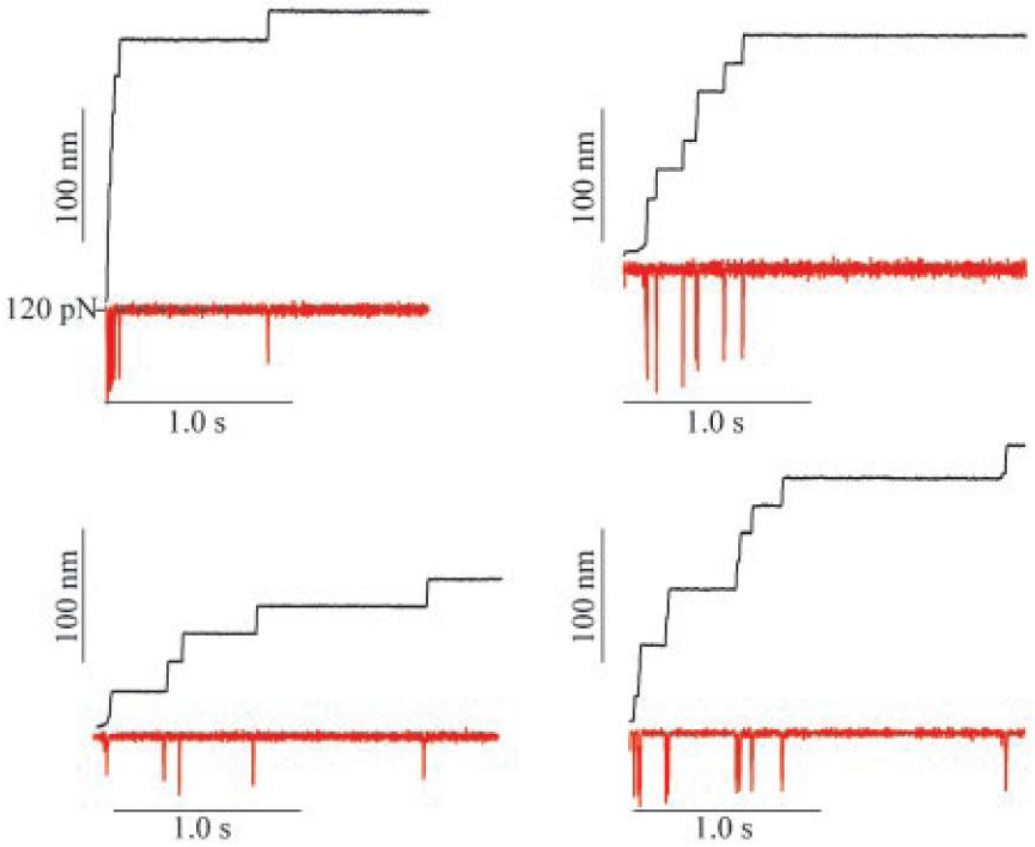

Figure 8: Unfolding of ubiquitin at a constant stretching force. The ubiquitin chains were stretched at a constant force of 120 pN (red traces) [30]

This thesis addresses the use of the AFM system combined with an electrostatic membrane actuator for lifetime experiments in biomolecules. The electrostatic membrane actuator will be characterized to demonstrate its capabilities. As shown before, because the biomolecules lifetime depends on the stretching force on the molecules [29], a feedback control system has to be used. This system should compensate for any changes in the force. The control system development will be shown and explained along with its algorithm. Lastly, the thesis demonstrates the feasibility of using this system for biological measurements.

CHAPTER II

MICROMACHINED MEMBRANE ACTUATOR

Electrostatically-actuated membrane devices have attracted a significant amount of attention, mainly due to their geometric simplicity and broad range of applicability in devices such as microphones [13], ultrasonic transducers [19], valves [12], and diaphragm pumps [12].

2.1 Structure and Operation

Electrostatic actuation (shown in Figure 9) is used by applying a voltage between the rigid bottom electrode and the flexible top electrode embedded in the membrane.

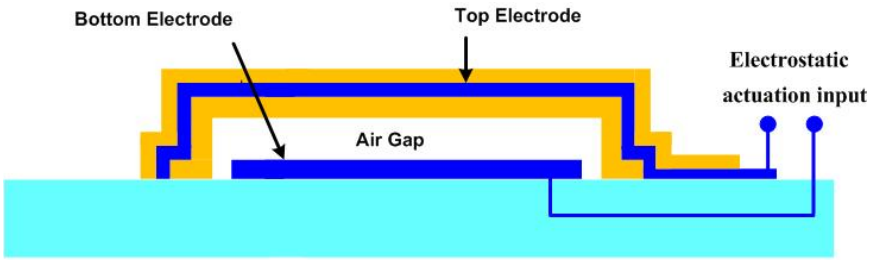

Figure 9: Schematic of an electrostatic membrane actuator.

By applying this bias voltage, opposite charges, $+Q$ and $-Q$ are formed on either side of the membrane. The membrane can therefore be modeled as a parallel plate capacitor with a movable upper plate. This model is illustrated in Figure 10.

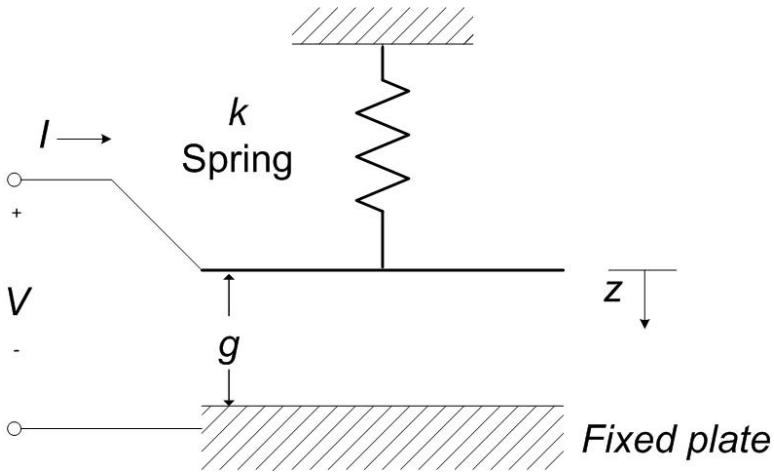

Figure 10: Basic illustration of an electrostatic actuator [31].

The charges on the opposite sides of the membrane attract one another according to coulomb's law [31]. This attraction force is determined by the electric field set by the opposite charges. This electric field is given by,

$$\varepsilon = \frac{Q}{\epsilon A} \tag{2}$$

where A is the area of the movable plate, and ϵ is the permittivity of the material in the gap between the two plates (hence $\epsilon = \epsilon_0$, the permittivity of free space). Therefore the attraction force can be expressed as the product of the electric field by the charge on the plates.

$$F = (\frac{Q}{2})\varepsilon = \frac{Q^2}{2\epsilon A} \tag{3}$$

Only half the charge on the plates is taken under consideration to avoid double counting [31]. The voltage on the plates can be found using Equation 4.

$$V = \frac{Q}{C} = \frac{Qg}{\epsilon A} \tag{4}$$

Where g is the gap between the two plates, and C is the capacitance of the membrane.

The energy in the parallel plate capacitor is therefore a function of both an electrical and a mechanical variables. This can be modeled using a two port capacitor which is shown in Figure 11.

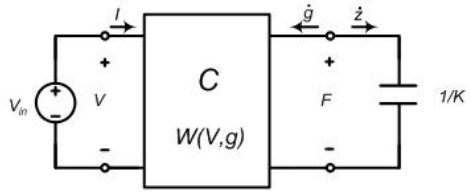

Figure 11: Voltage controlled electrostatic transducer [31].

The energy stored in this model can be written as,

$$W(Q, g) = \frac{Q^2}{2\epsilon A} \tag{5}$$

and the force and voltage can be expressed as the partial derivatives with respect to the gap (for the force), and charge (for the voltage). This model can also be used to find the relationship between the force, F, and the input voltage, V_{in} [31] which yields Equation 6.

$$F = \frac{\epsilon A V_{in}^2}{2g^2} + k(g_0 - g) \tag{6}$$

Where g_0 is the gap at zero volts and k is the spring constant.

2.2 Fabrication

The fabrication of these membranes was performed by Hamdi Torun, a PhD candidate at the MEMS labratory at Georgia Institute of Technology. The process was done on a 300 μm silicon wafer and used seven masks. Initially nitride was deposited on both sides of the wafer using PECVD, to allow both the back-side etching of the silicon wafer, and to isolate the bottom electrodes from the substrate. Mask one was used to create the bottom electrodes, which were made of gold and were deposited using the filament evaporator. Mask two was used to open an etching window on the back-side of the silicon wafer. Figure 12 illustrates the wafer after the two mask process.

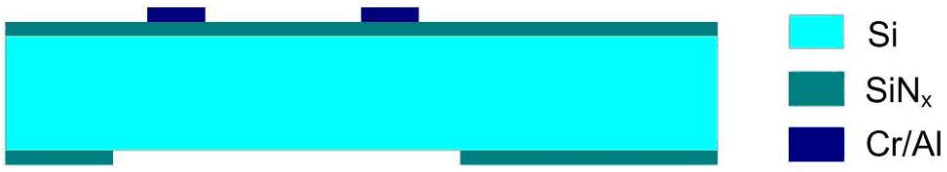

Figure 12: Bottom electrode deposition and back-side opening.

Positive photoresist (SC1827, Shipley) was spun on the wafer and patterned using mask three to create a sacrificial layer for the formation of the membrane structure. Figure 13 illustrates the membrane with the patterned sacrificial layer.

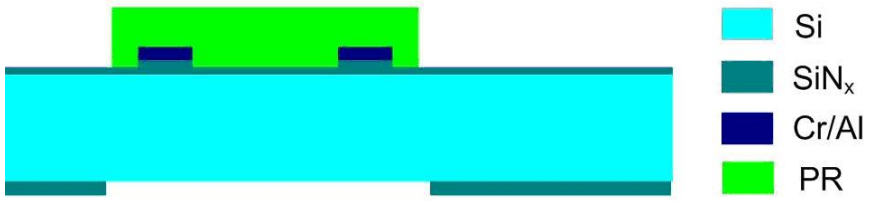

Figure 13: Sacrificial layer pattering for the membrane structure using mask three.

Once the sacrificial layer was patterned, a layer of parylene was deposited using CVD and patterned using mask four. This layer was used as an insulation layer between the top and bottom electrodes. The top electrode was then sputtered using

Aluminum and patterned using mask five in a wet-etching process. Figure 14 shows the membrane after these steps.

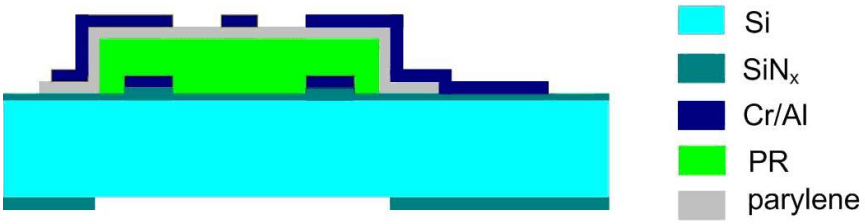

Figure 14: Top electrode deposition and pattering.

A final layer of parylene was then deposited over the top electrode and patterned using mask six. This layer insulated the top electrode from the fluid medium and prevented issues such as electrolysis which will be discussed later in this chapter. Mask seven was then used to open holes to the membrane connection pads trough the parylene layer. Figure 15 illustrate the deposition and patterning of the top parylene layer.

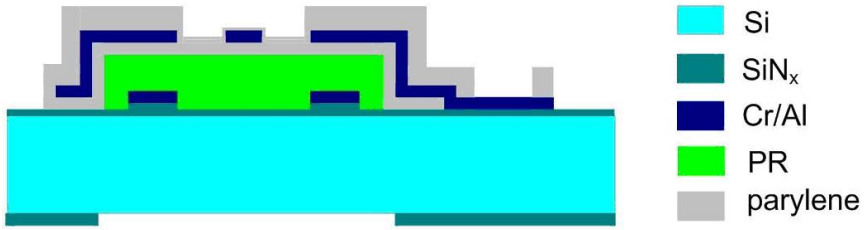

Figure 15: Deposition and patterning of the top parylene layer.

Once the parylene structure was complete, KOH etching was used to open the backside venting hole, which was opened initially using mask two. Finally the photoresist layer was removed and the membrane structure was released. The final membrane along with the different layer thicknesses is shown in Figure 16.

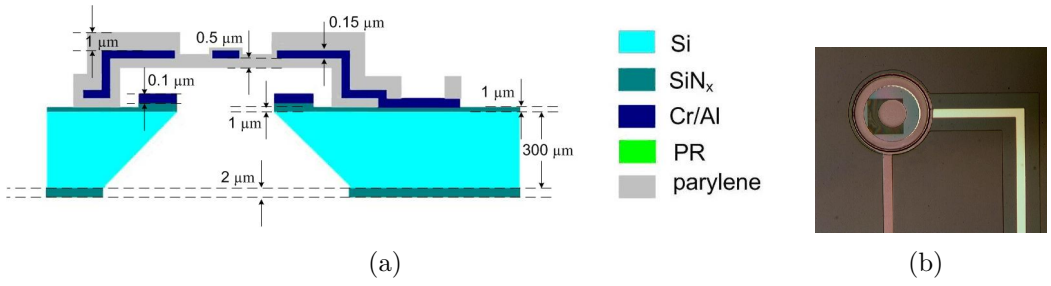

(a) (b)

Figure 16: (a) Released membrane with the different layer thicknesses. (b) Top side image of a 500 μm diameter parylene membrane.

2.3 Characterization

As was discussed earlier, the travel distance of the membrane has to accommodate for the full extension of the biomolecule. Therefore, when using an electrostatic membrane actuator, the pull-in instability has to be considered due to its limitation on the stable travel distance.

The voltage at the instability limit, also known as the "pull-in voltage", denoted by V_{PI}, is due to the electrostatic force increasing more rapidly than the spring force. Equation 7 shows the requirement for pull in voltage,

$$V_{PI} = \sqrt{\frac{8kg_0^3}{27\epsilon A}} \tag{7}$$

It is readily shown that the pull-in occurs at a distance, denoted by g_{PI}, and known as the pull-in gap. This value can be calculated using Equation 8.

$$g_{PI} = \frac{2}{3}g_0 \tag{8}$$

The actuation range is therefore set from the gap height to approximately one-third of the undeflected gap distance. This creates a limitation on the travel distance of the membrane, and prevents the full extension of the biomolecule. A method of increasing the actuation range will be discussed later in this chapter.

The membrane in AFM application was originally developed as a mechanical force

sensor known as the FIRAT probe [25]. The first version of the devices use aluminum membranes over an unsealed air cavity which made them unsuitable for biological experiments, which are done in liquid environments. The membranes are therefore required to be sealed in a dielectric material. A more suitable device for immersed operation, used in the experiments discussed in this thesis, has been realized using parylene (which is a biocompatible material) as the structural material [38]. Figure 17 shows an illustration of the parylene membrane structure

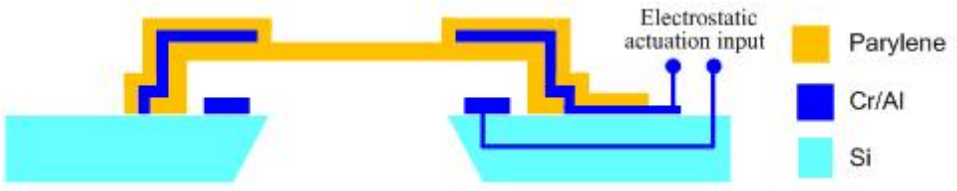

Figure 17: Illustration of the membrane actuator fabricated using parylene for the structural membrane.

Parylene, which is a relatively soft polymer (0.25 GPa), is deposited in a CVD under low pressure condition and at room temperature. The deposition process allows for accurate control of the deposited film, which can be deposited on virtually any available surface. By controlling the thickness of the membrane it is possible to adjust its stiffness which is an important characteristic.

As seen in Figure 17 the electrodes were buried in the dielectric membrane to electrically isolate them from the fluid medium. The backside of the membrane was etched to reduce the damping effect and allow faster actuation rates [39].

The devices were fabricated with a gap of 2500 nm and different diameter sizes ranges from 600 μm down to 200 μm. Figure 18 shows the measured cross section of a 500 μm membrane device which shows that the membranes are flat.

The variety of sizes will produce membranes with a range of different spring constants. These spring constants can be found experimentally using test systems such

Figure 18: Cross sectional profile showing a 2500 nm gap for a 500 μm diameter parylene membrane device.

as the TI 900 TriboIndenter (by Hysitron Inc.), which is ideal for measuring the hardness and elastic modulus of thin films and coatings. Figure 19 shows the results of the measured spring constant dependance on the diameter of the membrane (shown by the dots).

The spring constant is an important parameter for the membrane structures, denoted by k, which determines the membrane's stiffness. The lumped model prediction, which is shown in the figure, is found using Equation 9, which is the characteristic equation for a flat circular diaphragm, connected at the edges, for small displacements [5].

$$\frac{Pa^4}{Eh^4} = \frac{16y}{3(1-\nu^2)h} + \frac{(7-\nu)y^3}{3(1-\nu^2)h^3} + \frac{4a^2\sigma y}{(1-\nu)Eh^3} \tag{9}$$

Where h is the thickness of the diaphragm, E is the Young's modulus, a is the radius of the diaphragm, ν is the Poisson's ratio, and σ is the biaxial residual stress. The figure shows discrepancies between the model and the experimental results in both the smaller and larger size membranes. In the smaller size membranes the discrepancies may arise due to the fully clamped support boundary which is assumed by the model. This assumption does not hold in the experimental results due to a

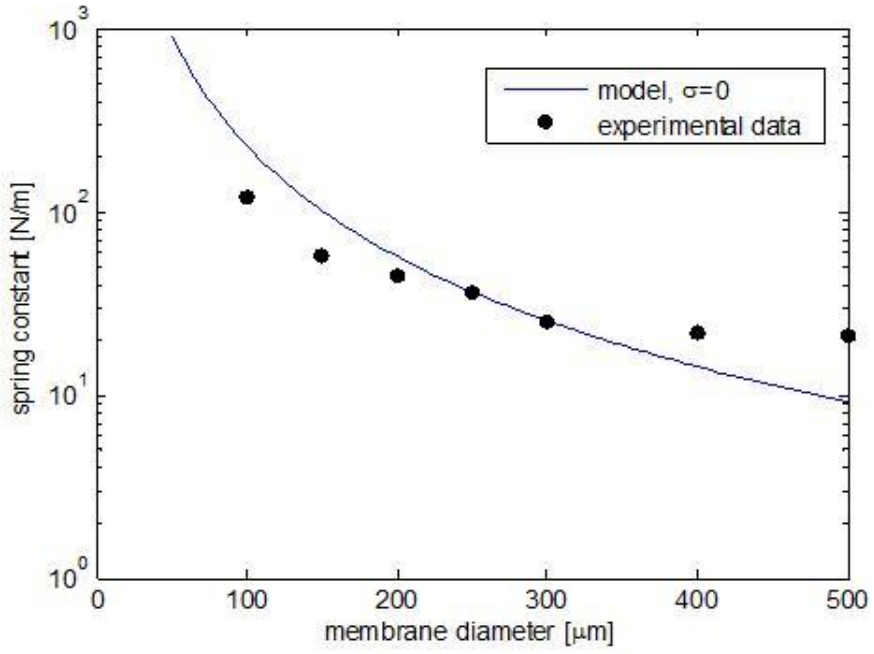

Figure 19: Measurement of spring constant of fabricated parylene membranes (courtesy of Hamdi Torun).

difference in thickness between the membrane's side wall and the membrane's actual thickness. In the larger size membranes the discrepancies with the model may arise due to residual stress which dominates the spring constant, and as seen in the figure, increases the membrane's spring constant above the values predicted by the model.

Equation 10 demonstrates how the spring constant value can be calculated at a specific voltage and at a gap which corresponds to that voltage.

$$k = \frac{\varepsilon A V^2}{g^3} \tag{10}$$

To avoid electrolysis issues in biological experiments (which will be discussed later in this thesis), additional layer of parylene were deposited on the membrane. Changing the thickness of the membranes increases their stiffness and spring constant which changes the characteristics of the membrane. Figure 20 shows the change in spring constant value as a function of both membrane diameter and membrane thickness.

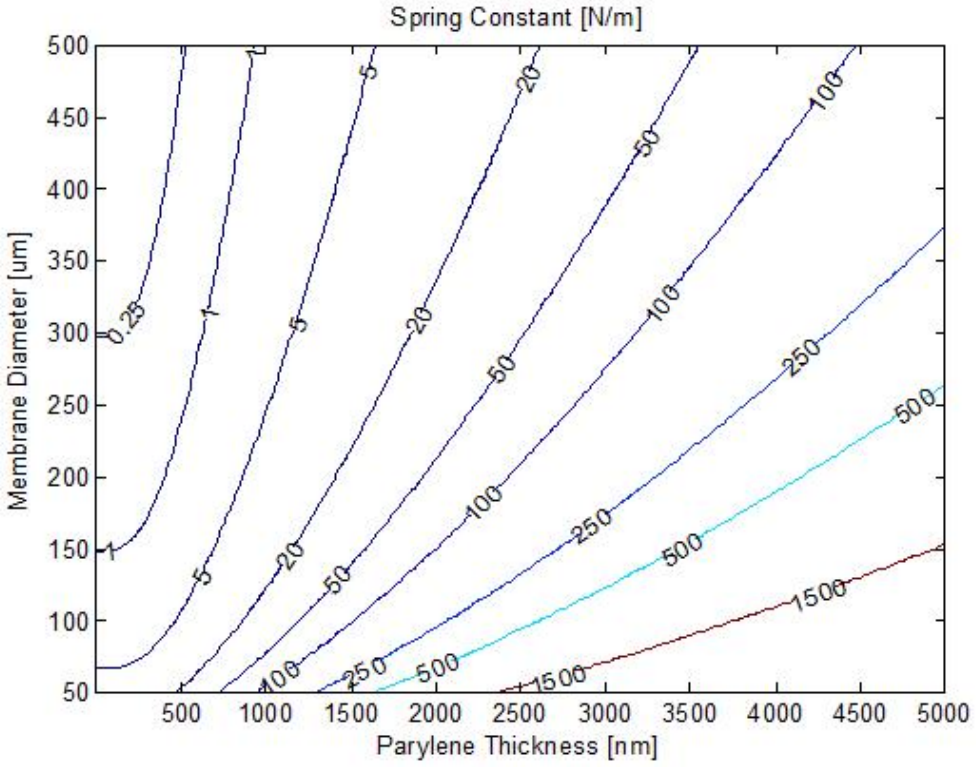

Figure 20: Calculated spring constant of fabricated parylene membranes.

The figure clearly shows that as the thickness of the membrane increases the stiffness of the membrane increases as well. The spring constant of a 360 μm membrane, used in the experiments discussed here, was found to be 60 $\frac{N}{m}$ after the additional deposition of 2 μm of parylene (total thickness of 3.5 μm), which is in agreement with Figure 20.

During the experiments that will be discussed, the force sensing cantilever was placed above the membrane as shown in Figure 21.

Because the membrane is used as the actuator its displacement has to be controlled at all time and should not be interfered by the cantilever which is placed above it. Therefore, the membrane has to be significantly stiffer as compared to the cantilever.

The cantilevers used in these experiments have a spring constant ranging between 1 $\frac{N}{m}$ to 0.01 $\frac{N}{m}$. These values are significantly smaller than the spring constant of the

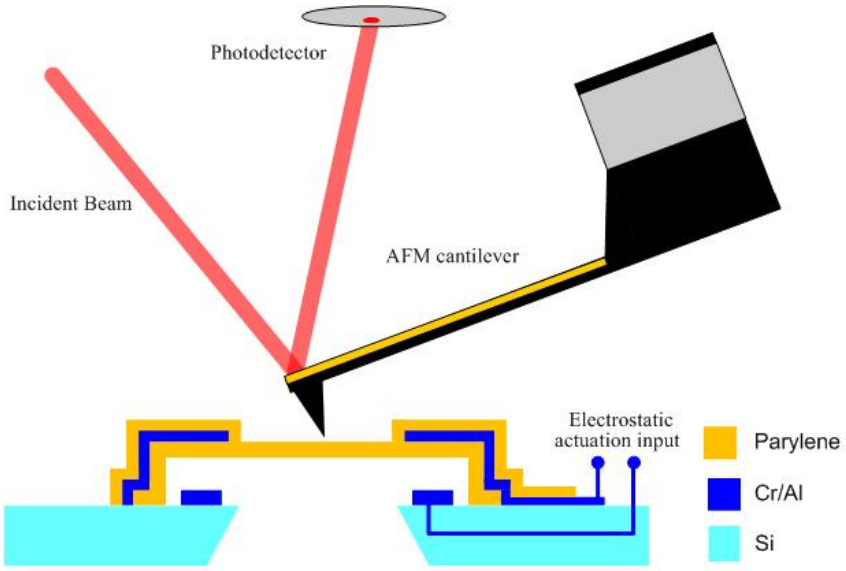

Figure 21: Illustration which shows the location of the cantilever with respect to the membrane.

membrane and therefore the membrane can be considered rigid as compared to the cantilever.

2.3.1 Static Actuation Range

As mentioned earlier, for the purposes of these experiments, it is desirable to try to increase the range of electrostatic actuation beyond the one-third of the gap length. By placing electrodes close to the clamped edges (see Figure 22) it is possible to apply electrostatic force only to that specific area of the membrane. This method,

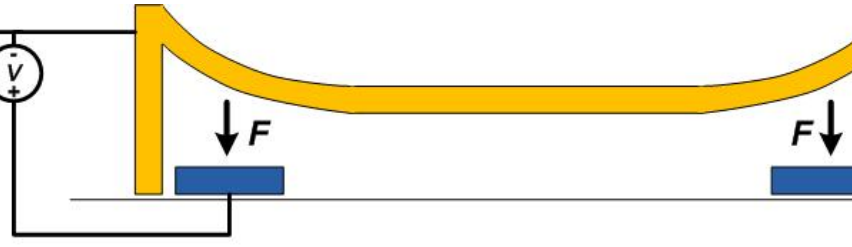

Figure 22: Membrane fabricated with only side electrodes for its bottom electrode. The leveraged bending method allows the center of the membrane to travel a larger distance before pull-in will occur.

also known as the leveraged bending, allows the center of the membrane to travel a larger distance before pull-in will occur in the electrostatically actuated portions [15].

Table 1 shows the different membrane diameters, fabricated for the experiments discussed in this thesis, and their corresponding side electrode boundaries.

Table 1: Device Dimensions

Membrane and electrode outer diameter(μm)	Inner diameter (μm)
600	240
500	300
400	300
400	200
360	240
350	175
300	120
200	120

The membrane diameter is also the outer boundary of the bottom electrode, while the inner diameter shows the inner boundary of the electrode.

Figure 23 shows data obtained from the 360 μm membrane used in the experiments.

The data illustrates the relationship between the deflection of the membrane and the applied voltage on the membrane. As mentioned before the gap of the membrane is approximately 2500 nm, which means that the regular limit is at 830 nm (denoted in Figure 23 by the horizontal line). It is clearly seen that by placing the bottom electrodes next to the support beams, it is possible to deflect the membrane beyond the initial pull-in limit to more than two-thirds of the membrane gap.

Within this range it is possible to actuate the membrane fast since the speed is only limited by the membrane dynamics and is not affected by the fluid. It was found that a third order polynomial fits best to this relationship. This polynomial can be inverted in fast pulling experiments to effectively suppress the system nonlinearity, which is inherent in electrostatic microactuation systems.

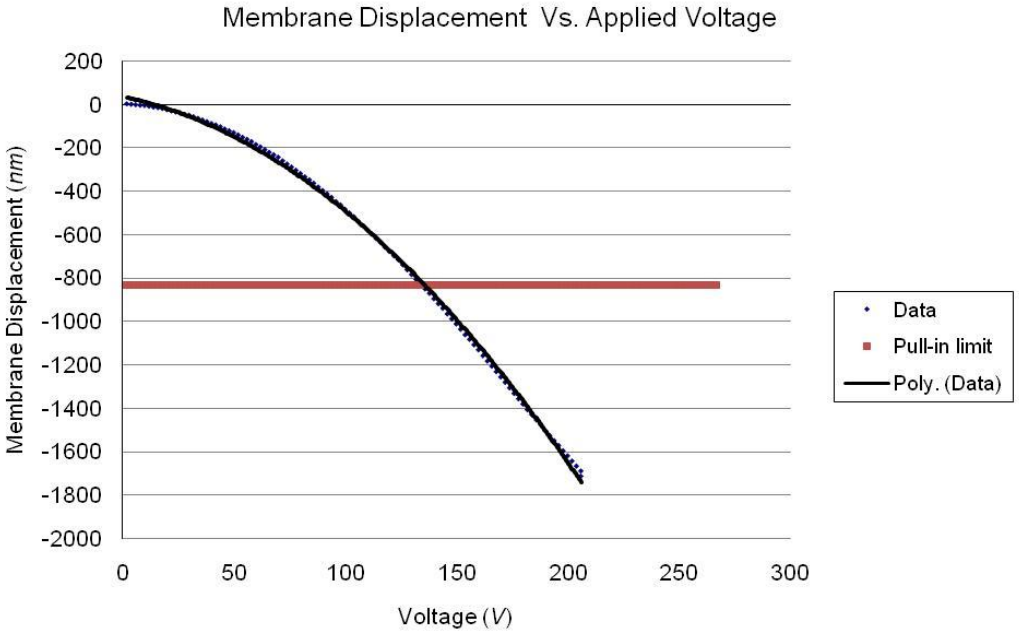

Figure 23: Calibration curve for the 360 μm membrane. The curve shows the displacement of the membrane (nm) as a function of voltage. The zero displacement value indicates the full gap of the membrane.

This nonlinearity makes the membrane control more difficult. For example, when a voltage ramp signal is applied to the membrane, a non-linear displacement is obtained as seen in Figure 23. This behavior can be explained using Equation 6 which clearly shows that the relationship between the membrane's voltage and membrane's displacement is non-linear. To effectively overcome the system nonlinearity and obtain the desired system response, the polynomial fit (obtained by the membrane's voltage, displacement relationship) was used as a "black box" conversion tool. Figure 24 demonstrates how the "black box" conversion process was performed.

2.3.2 Dynamic Actuation

Since one of the important goals of the project is to increase actuation speed, membrane dynamics are very important. Figure 25 shows the measured frequency response of the 360 μm membrane used in the experiments.

The frequency response was obtained by biasing the membrane at 70 V, DC

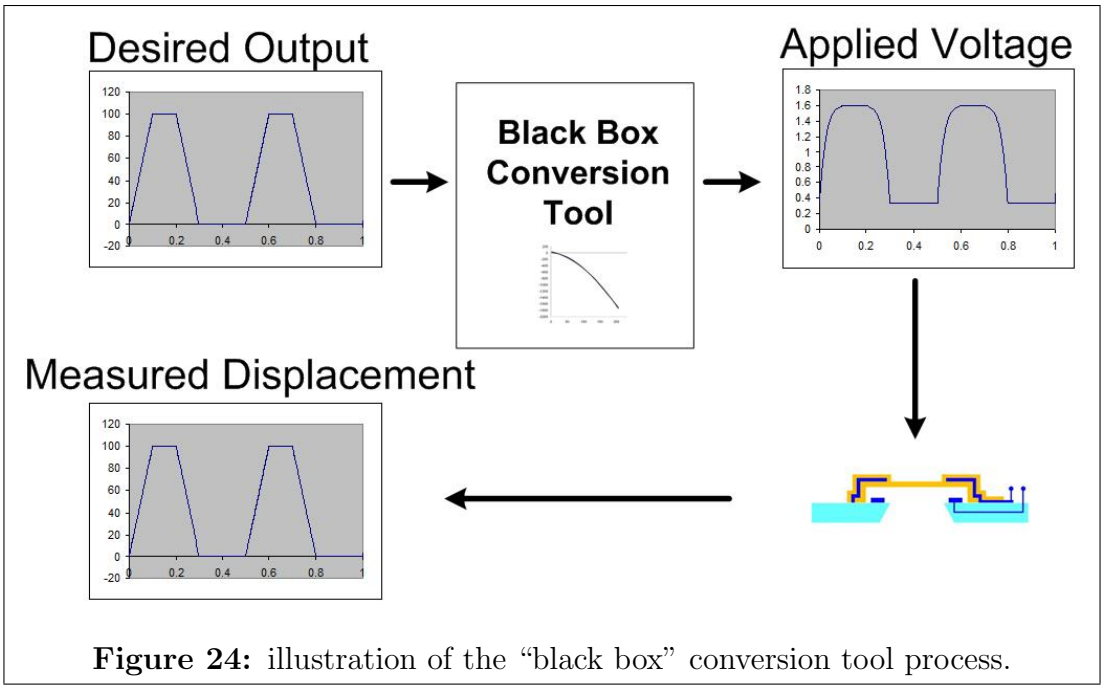

Figure 24: illustration of the "black box" conversion tool process.

voltage, and applying a $+5V$ peak-to-peak sinusoidal signal at different frequencies. The displacement amplitude for the different frequencies was measured using backside diffraction-based optical interferometer [38].

Figure 25 shows a frequency response of 100 kHz in air which is a significant improvement to the actuation bandwidth when compared with the actuation bandwidth possible with a typical piezoelectric actuator which ranges between 1 kHz to 2 kHz. When the membrane is immersed in fluid the bandwidth reduced to 10 kHz, which is also considerably larger than the typical piezoelectric actuator.

2.3.3 Non-Ideal Behavior

2.3.3.1 Electrolysis

During biological experiments the membrane is entirely immersed in a buffer medium which is a conducting liquid. Therefore the top electrode, which is located in the parylene structure, must be insulated from the liquid medium (in this case the parylene acts as the insulating medium). This is done in order to avoid electrochemical processes such as electrolysis which can damage uninsulated areas on the membrane.

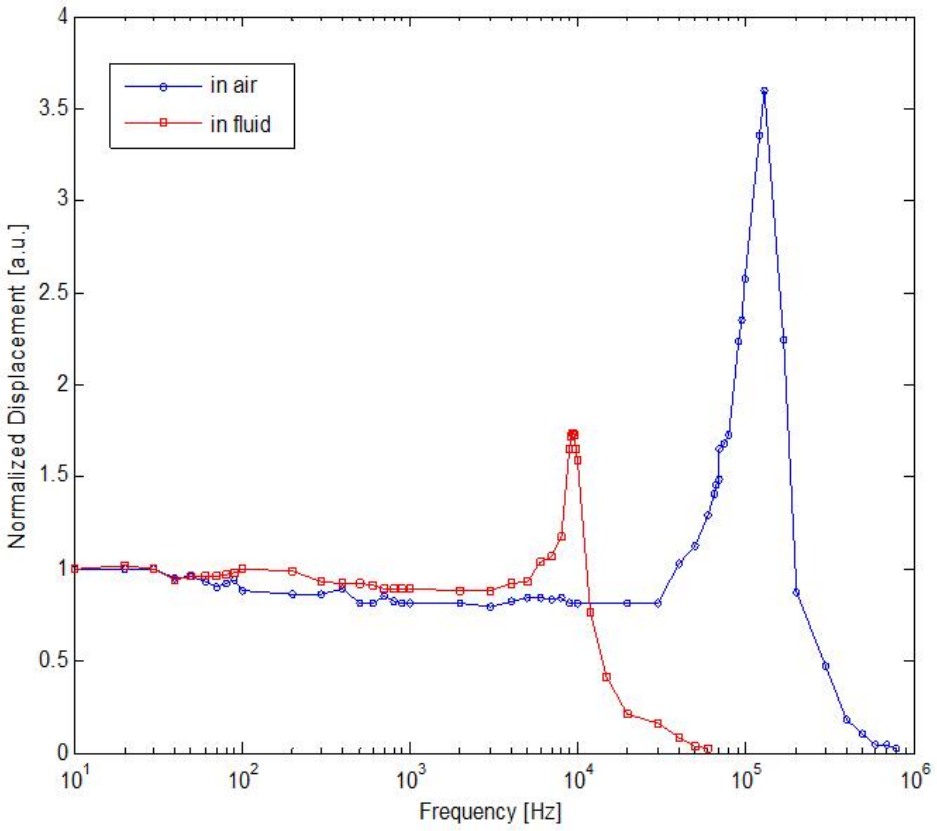

Figure 25: Frequency response of a 360 μm diameter membrane used in the experiments described in these thesis [38].

Such damage can lead to failure either from a slow degradation of the actuation ability of the membrane or in some cases bubbles that will be formed on the actuator portion of the membrane. Electrolysis is described as the decomposition of some components in a solution by the passage of an electrical current through the solution. In order for electrolysis to happen continuously a minimum voltage, also known as the theoretical decomposition voltage, has to be reached. This voltage must be at least slightly greater than 1.28 V [11]. To further avoid electrolysis in the experiments, the top electrode, which is buried in the membrane structure, was biased to ground.

Ideally parylene should be enough in order to avoid electrolysis but the floating potential in the liquid medium can exceed the 1.28 V threshold, resulting in electrolysis. A second layer of parylene was deposited on top of the membrane to prevent this electrolysis.

2.3.3.2 RF Modulation

A different method of preventing electrolysis is by driving the membrane using a high frequency modulation signal. To achieve force modulation, a sinusoidal AC force is superimposed on the desired signal. Where the voltage applied to the membrane will be composed of the product of the square root of the desired signal and an AC voltage. Because the electrostatic force generated is proportional to the square of the applied voltage, as seen in Equation 6, the final signal will be the desired signal. Mathematically this can be shown by using an input voltage signal with a certain frequency, denoted by $V(t)$ which is superimposed with a high frequency AC signal, $cos(\omega t)$. Because $V(t)$ is proportional to the square root of the electrostatic force, $\sqrt{F(t)}$ is used instead of the voltage.

$$[V(t)cos(\omega t)]^2 = [\sqrt{F(t)}cos(\omega t)]^2$$
$$= F(t)\tfrac{1}{2}[1 + cos(2\omega t)]$$
$$= \tfrac{F(t)}{2} + \tfrac{F(t)}{2}cos(2\omega t)]$$

The frequency denoted ω is much larger than the frequency response of the membrane and from the frequency of $\sqrt{F(t)}$. Therefore, the second term which contains ω can be neglected. The only term left is $\frac{F(t)}{2}$ Which shows that using the frequency modulation signal it is possible to achieve the desired electrostatic force on the membrane without the use of a DC voltage.

Figure 26 illustrates the desired membrane displacement signal (shown in 26(a)). This signal was converted to a voltage signal, using the conversion method discussed earlier, and superimposed with a high frequency AC signal to produce the modulated membrane voltage shown in 26(b). Applying this voltage signal to the membrane

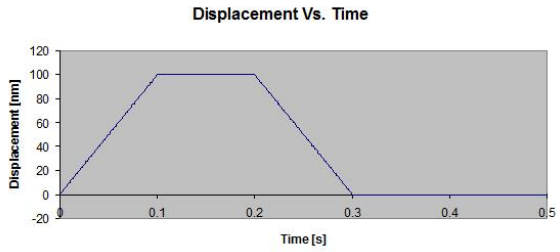

(a)

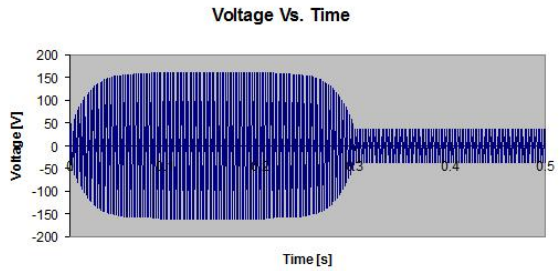

(b)

Figure 26: (a) Original ramp signal inputted by the user. (b) Modulated signal inputted to the membrane.

should produce the desired membrane displacement signal. Figure 27 shows a closer look to the modulated signal shown in Figure 26.

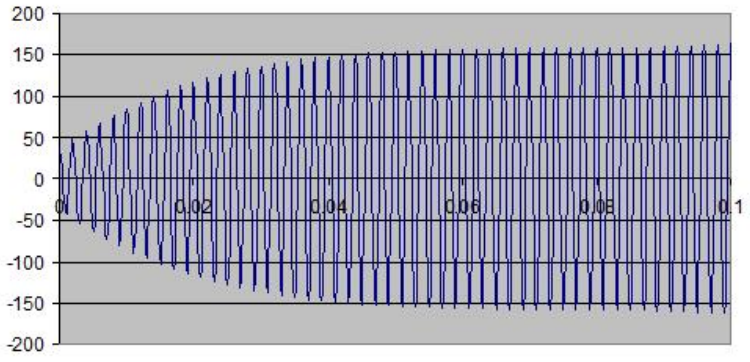

Figure 27: Closer look of the modulated signal shown in Figure 26.

Electrolysis should not occur because the average voltage on the membrane is approximately zero, and as mentioned earlier, in order for electrolysis to occur the average voltage on the membrane has to be slightly larger than 1.28 V.

CHAPTER III

EXPERIMENTAL SETUP AND CONTROL SYSTEM

This chapter describes the different components which were used in the force spectroscopy experiments along with a discussion on the development and operation of the control system.

3.1 Setup Components

The experiments were performed using a Dimension 3100 AFM system which was placed on TMC pressurized table (see Figure 28)

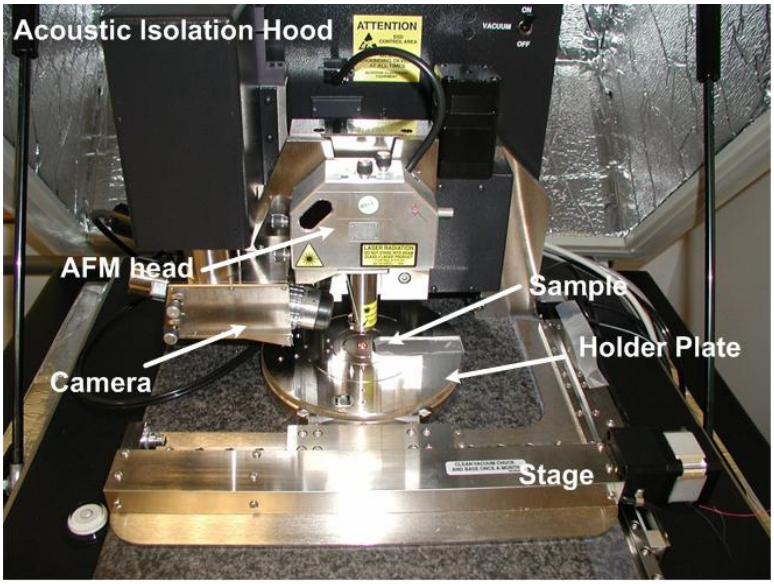

Figure 28: Dimension 3100 AFM system.

A 320 μm long, triangular-shaped cantilever made of silicon nitride, chromium and gold (MLCT-C, Veeco Probes) was used as the force sensing cantilever. The spring constant of the cantilever was approximately 0.01 $\frac{N}{m}$ and its resonant frequency was around 7 kHz in air. Figure 29 shows the schematics along with an image of the actual cantilever.

The cantilever was placed on a fluid cantilever carrier, using the carrier holder, and mounted on the piezo head. Figure 30 illustrate this step.

The membrane chip containing several of the membrane structures was mounted on a printed circuit board, also known as PCB, using epoxy material. Figure 31 shows

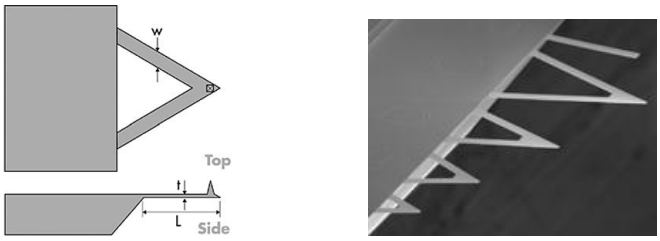

(a) (b)

Figure 29: (a) Cantilever schematics. (b) MLCT-C, Veeco cantilever (images were taken from the Veeco Probes website).

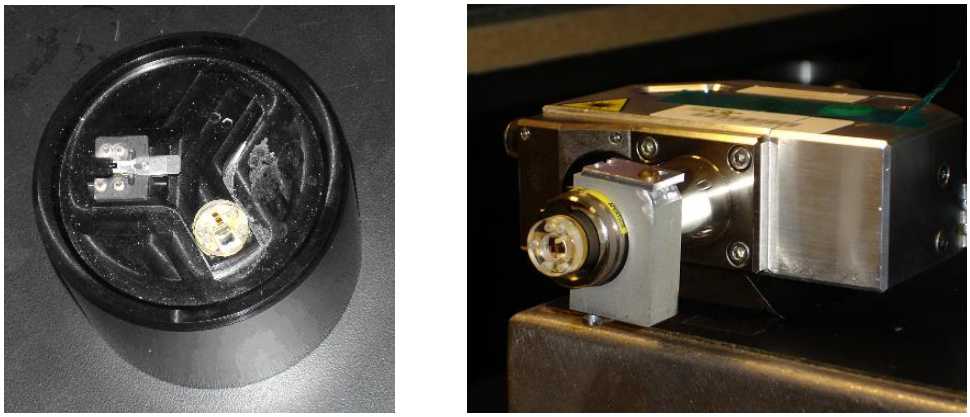

(a) (b)

Figure 30: (a) Cantilever placed on a fluid cantilever carrier using the carrier holder. (b) Cantilever is mounted on the AFM piezo head.

the membrane chip mounted on the PCB board.

Using a wire bonder the PCB was interfaced with the membrane connection pads. The connections to the PCB allow for an easier interface with the system's control panel which will be discussed later in this chapter. The PCB was then loaded onto the AFM holder plate and placed at the sample location (see Figure 28). It is important to note that the maximum clearance between the holder plate and AFM head is 21 mm (when the AFM head is fully retracted). Therefore, the sample thickness has to be thinner than 21 mm. Figure 32 shows schematics of the dimensions of the holder plate with respect to the piezo head.

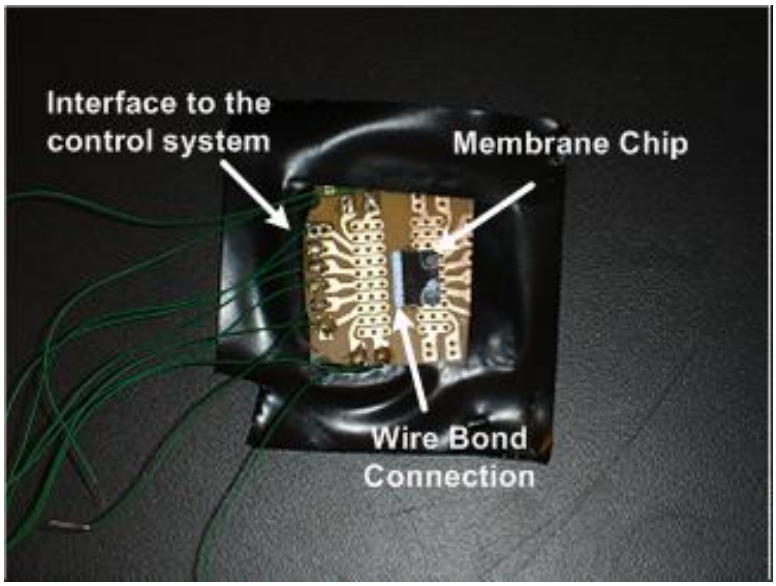

Figure 31: Membrane chip mounted on PCB.

For experimental verification of this system with biomolecules, human and anti-human IgG molecules were used. 10-20 μl of anti-human IgG was incubated on the membrane while 10 μl of human IgG was incubated on the AFM cantilever. The incubation process was done over night at room temperature. The biomolecules are required to stay in fluid at all time. Therefore, when the incubation period was over, additional dulbecco's phosphate buffered saline (also known as DPBS) was added, as necessary, to ensure the biomolecules were in fluid. Because the addition of the buffer was done after the incubation time, the molecule concentration was not diluted. After the buffer solution was added to the sample and cantilever, to keep the molecules in fluid at all time, the cantilever was engaged on top of the membrane and the experiments started (see Figure 33 for an illustration).

The acquisition and the generation of the physical signals of the microcontroller have been performed by 16-bit, National Instruments multifunction Data Acquisition (DAQ) board (NI PCI 6229) connected to the user's PC. The detailed specification of this card is given in Appendix D. The DAQ card is limited in both its input and output voltages with values in the range between -10 V to 10 V. In order to

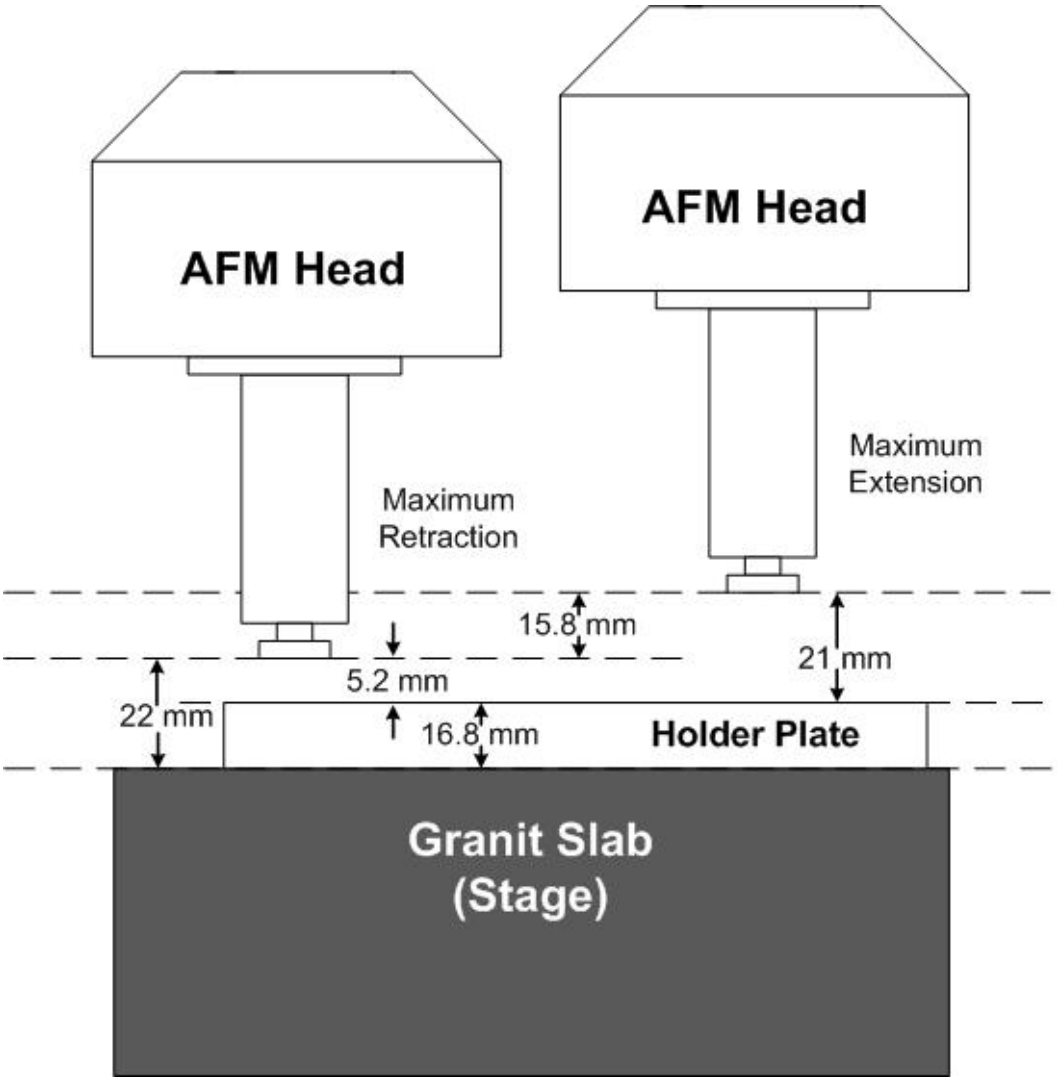

Figure 32: Schematic drawing illustrating the dimensions of the Dimension 3100 AFM sample stage with respect to the piezo head.

use the DAQ card to actuate the membrane, voltages above 10 V were needed (as seen by Figure 23) , which requires the use of an additional amplifier. The DAQ card was connected to a BNC-2110 connector box (National Instruments). A layout schematic of the connector box is given in Appendix E. The input connector, $ai0$, on the connector box was connected to the photodiode output on the signal access modules, also known as SAM. The SAM is a device that allow access or interruption of signals between the AFM Dimension system and its controller. Using this device

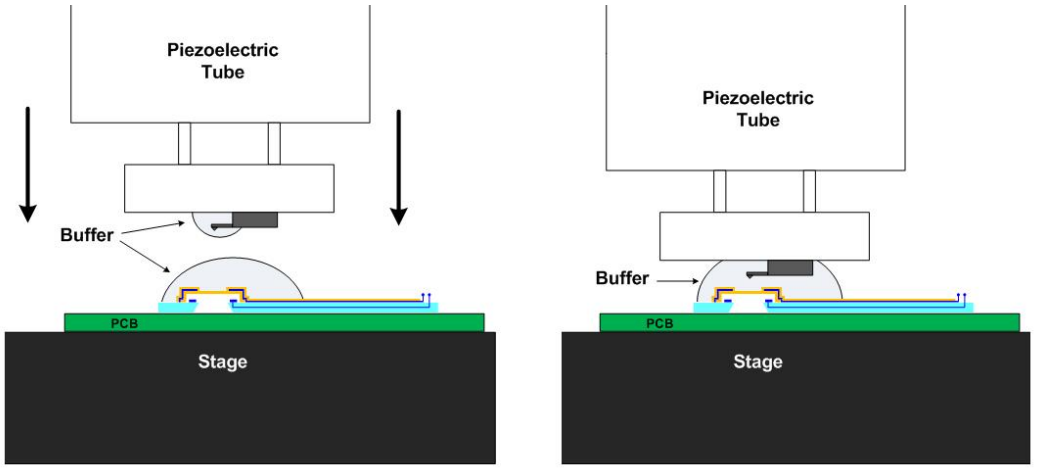

Figure 33: The experimental system after the biomolecules were incubated on both the cantilever and membrane. The cantilever is then engaged on top of the membrane.

signals can be injected, tapped, and modified as they flow between the AFM detection system and the controller.

As mentioned earlier in order to amplify the signal the output connector, $ao0$, on the connector box, was connected to a E-507 Amplifier Module (HVPZT, Physik Instrumente) which has a single-channel values of between 3 V to 1100 V output range. The piezo amplifier was directly connected to the membrane. Figure 34 illustrates how all the devices in the experiment were connected.

For the development of the control software, National Instruments LabVIEW 8.5 was used to control the membrane using the data obtained from the AFM system. The program also allowed the user to control the experiment by giving him an easy to use interface access to input the different parameters.

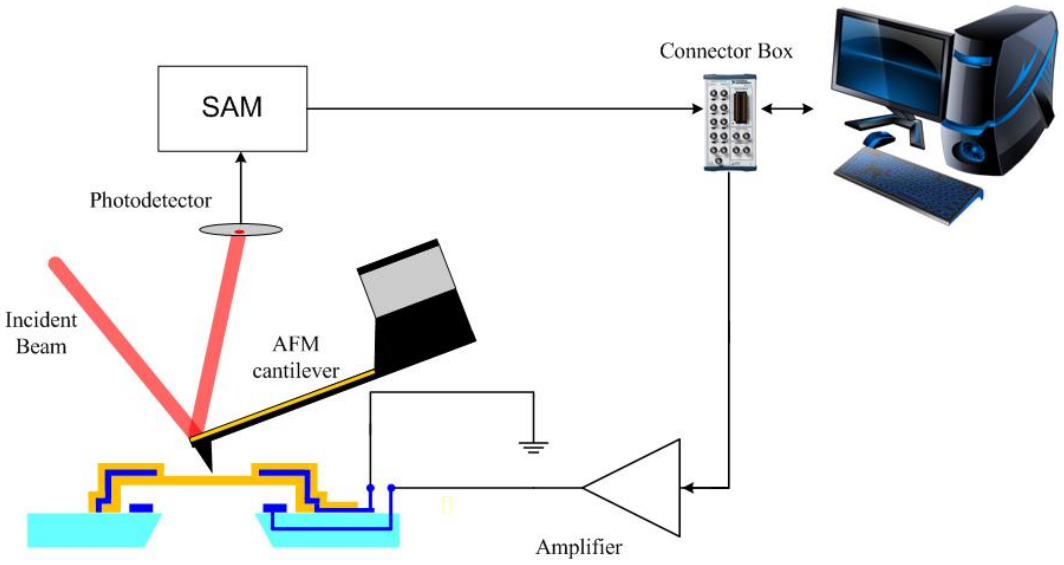

Figure 34: Block diagram which illustrates how all the different devices in the control system were connected.

3.2 Drift

When designing the control system for the force spectroscopy experiments, the motion of the cantilever has to have a "fixed" relationship to the membrane. This relationship is determined by the user, and should be maintained throughout the experiment. In force-clamp experiments this relationship is determined by the force on the biomolecule while in the loading rate experiments the relationship is determined by the distance between the membrane and the cantilever. Figure 35 shows the drift during an experiment over the time period of 6 minutes.

Drift might be the result of different components in the control system. These components include cantilever drift, piezo drift, and membrane calibration shift.

- **Cantilever drift -** Most drift has been attributed to the asymmetric geometry of the cantilever, which acts as a chemical and thermal bimorph. The time course of drift is roughly exponential with a time constant of $\sim$70 *min* [4]. This issue will have a more significant effect in low loading rate experiments and low force force-clamp experiments, mainly because the lifetime value for the

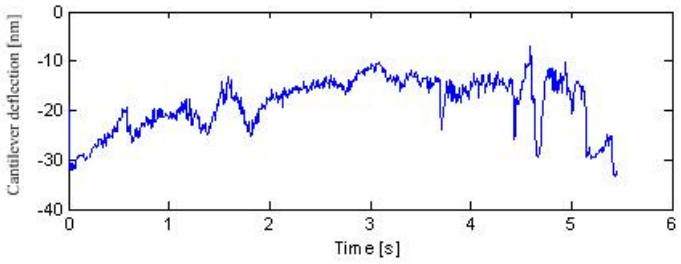

Figure 35: Drift during a biological experiment.

biomolecule bond, as was discussed earlier, can be larger.

- **Piezo drift -** To maintain high accuracy, the Dimension 3100 requires the piezo to be calibrated every three-to-four months [6]. This shows that the piezo drift should also be taken under consideration.

- **Membrane calibration shift -** This might be the result of charge build up or membrane plastic deformation. Figure 36 shows the displacement as a function of voltage, on the same membrane, at different times during the experiment. The shift in calibration values is clearly shown.

Drift is therefore very important and needs to be considered mainly for the force-clamp experiments which require constant force at all time. To avoid the drift problem, a feedback control should be used which should compare the output force from the photodiode system with the desired value that the user inputted. The program will compare each point in real time and compensate for the difference if needed. This change can be done by either changing the displacement of the piezo head, or by changing the displacement of the membrane. This system uses the cantilever as a force prob only, and the membrane as the actuation device. Therefore, the force will be maintained at a constant value, at all time, by changing the position of the membrane. This will allow the program to compensate for any changes caused by

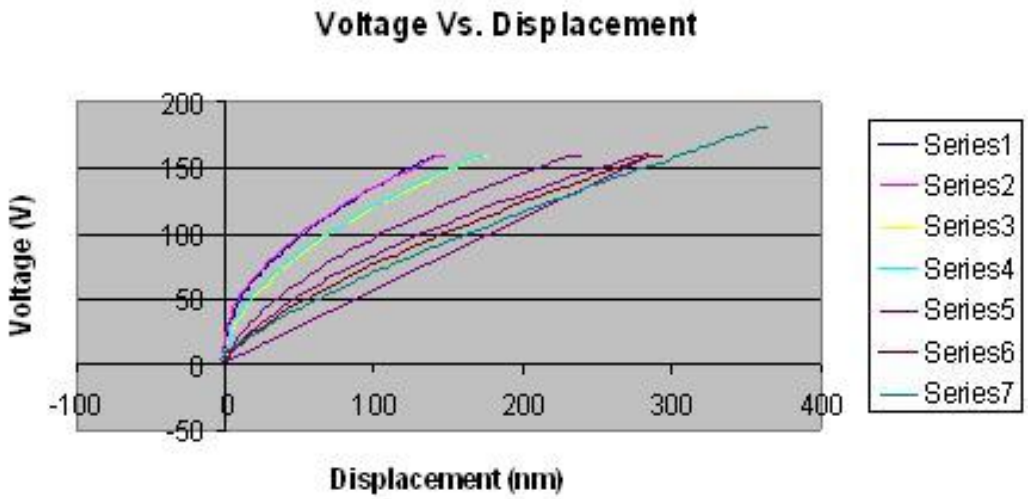

Figure 36: Calibration curve as were taken at different period of time in the experiment.

drift or plastic deformation of the membrane.

3.3 Control System Development

For the experiments performed by this system a control scheme was developed to measure and characterize the intramolecular forces. When the tip of a flexible silicon nitride cantilever is brought in contact with the surface, random binding could occur between the protein molecule and the tip atoms. If the other end of the molecule is immobilized to the surface (membrane in this case), the protein can be stretched by increasing the distance between the cantilever and the surface. Forces were measured by detecting the deflection of the cantilever onto which the beam of a laser diode was focused. The reflected beam illuminates a photodiode, which records a differential signal that was fed back into the program. Using the spring constant and sensitivity of the cantilever, which are found at the beginning of the experiment, it was possible to convert between the photodiode output voltage (V) to the deflection of the cantilever tip (nm). Eventually these quantities allowed us to find the force, F (pN), on the sample by using the spring constant of the cantilever (pN/nm) which was a given characteristic of the cantilever.

Two control schemes were considered for this system. The first one, which involved the loading rate experiments, was an open loop system. This control scheme performed a calibration test on the membrane at the beginning of the experiment. The calibration data was stored and then used as a conversion tool to linearize the membrane motion for different loading rates. Figure 34, which was shown earlier in the chapter, can be used to illustrate this control system scheme. The figure might show a close loop system but this is only at the beginning of the experiment when the calibration data was obtained. The voltage output to the membrane repeats itself with no change, and therefore this can be considered as an open loop system. The advantage of using this control system over other methodologies such as signal function generator, which can also create a continues ramp signal, is that using this control system the user can create a complex signal which involves different loading rates.

The second control scheme, which was designed for the force-clamp experiment, was a closed loop (feedback loop) system which was required to maintain the force on the biomolecule at a constant value. Figure 38 can be used to illustrate this control system scheme.

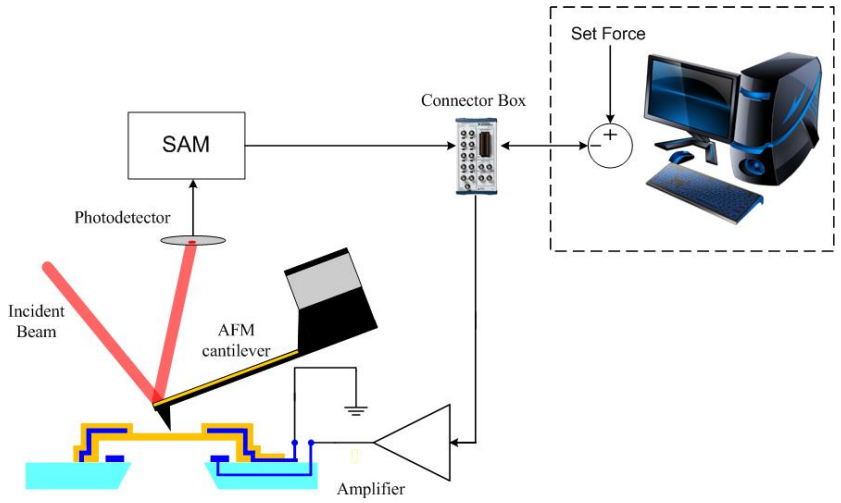

Figure 37: Illustration of the control system used in the force-clamp experiments.

The figure shows the control feedback system incorporated as part of the computer processing box. The feedback compares the force value, at all time, and adjust the membrane voltage accordingly, to maintain a constant force value.

As was discussed earlier, when implementing this system for the purpose of loading rate experiments there is no need for a feedback system, which significantly lowered the complexity of the program. Appendix B.1 illustrates the program developed along with its operating instructions. By specifying a displacement signal in nm, and using the voltage-displacement relationship, the displacement values were converted to voltage and applied to the membrane. The signal would be repeated continuously until the user would decide to terminate it. During this time the displacement of the cantilever (nm) was captured and stored into a $.xls$ file. For reference purposes the original displacement signal to the membrane was also stored on the same file.

As mentioned earlier, force-clamp experiments require a feedback system which

add a degree of complexity to the control scheme. Figure 38 shows a flow chart illustrating the programs algorithm for the force-clamp experiment.

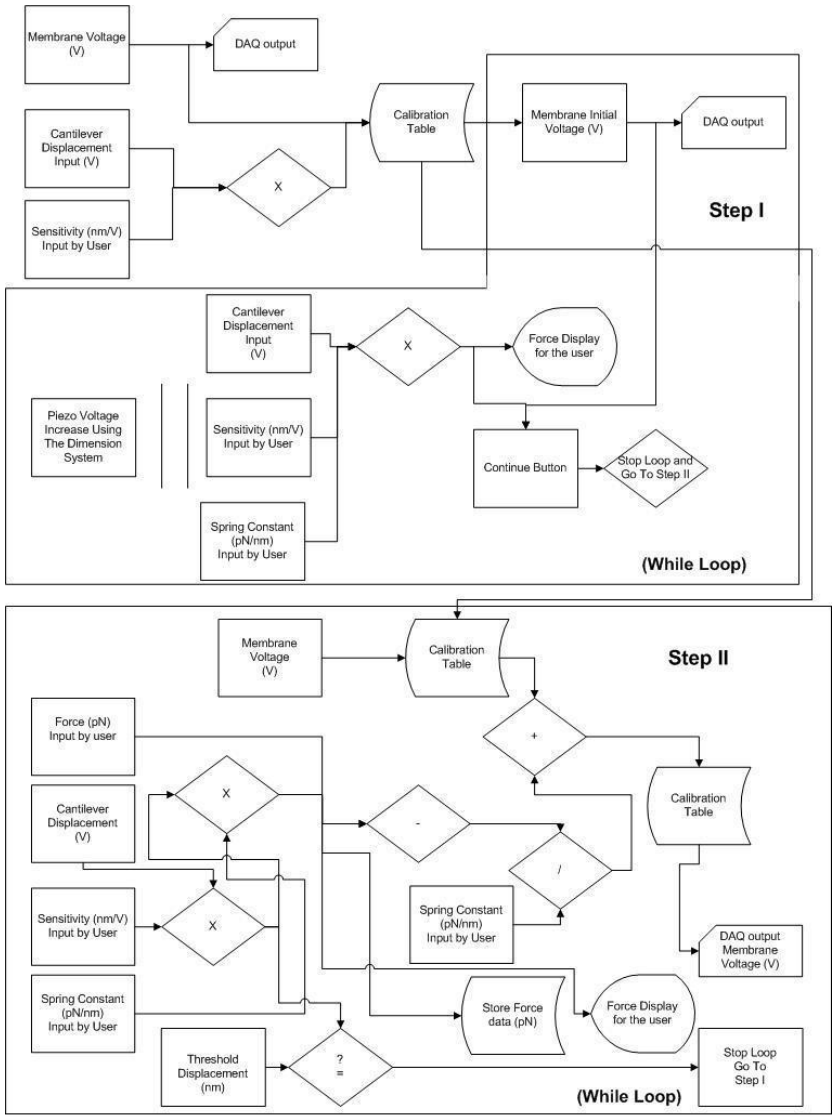

Figure 38: Flow chart illustrating the programs algorithm.

The algorithm operates by going back and forth between two different states, denoted as *Step I* and *Step II*. Initially, before going into *Step I*, a calibration process is performed on the membrane in order to find its voltage (V), displacement (nm) relationship. This information is stored in a calibration table array and saved in a *.xls* file. In pulling experiments this data can be used to linearize the membrane's

motion (see section 2.3.1).

The force on the molecule will be controlled from the membrane side. Because the membrane should have the capability of negative displacement to allow the reduction of excess force, an initial voltage will be applied to the membrane. This voltage will be reduced when needed, to allow an upward displacement of the membrane actuator. The membranes displacement is shown to be larger than 1000 nm (Figure 23), which corresponds to a force range of over 10,000 pN. The DAQ card does not allow writing to two channels simultaneously, which prevent the control of the piezo using the LabVIEW program. Instead, the process can be done manually by using the "*step up*" option of the motor control, in the dimension system. The force will be shown on the front panel of the display and can allow the user to set the force to any inital value. The user then presses the continue button which moves the program to the next step. In *Step II* the force is continuously monitored and compared with the specified force. Any changes to the force are obtained by changing the membrane's voltage. This process is illustrated in Figure 39.

As seen in the figure, only the displacement of the cantilever tip, shown by the triangular shape, is considered. The higher the position of the cantilever tip, the higher the voltage output from the photodiode (shown in Figure 39 (a)). If the cantilever tip moves down, a drop in the photodiode voltage is detected (force decreases). The membrane voltage will therefore increase, causing an increase in the membrane's displacement and shifting it downwards (shown in Figure 39 (b)). In the other case, if the cantilever tip moves up, an increase in the photodiode voltage is detected (force increases). The membrane voltage decreases, decreasing the membrane's displacement, and shifting it upwards (shown in Figure 39 (c)). In case the displacement of the cantilever passes a threshold value, specified by the user, the program assumes a rupture event has occurred and moves back into *Step I*. By doing so, it allows the program to repeat the experiment. All of the force (pN) as a function of time (s)

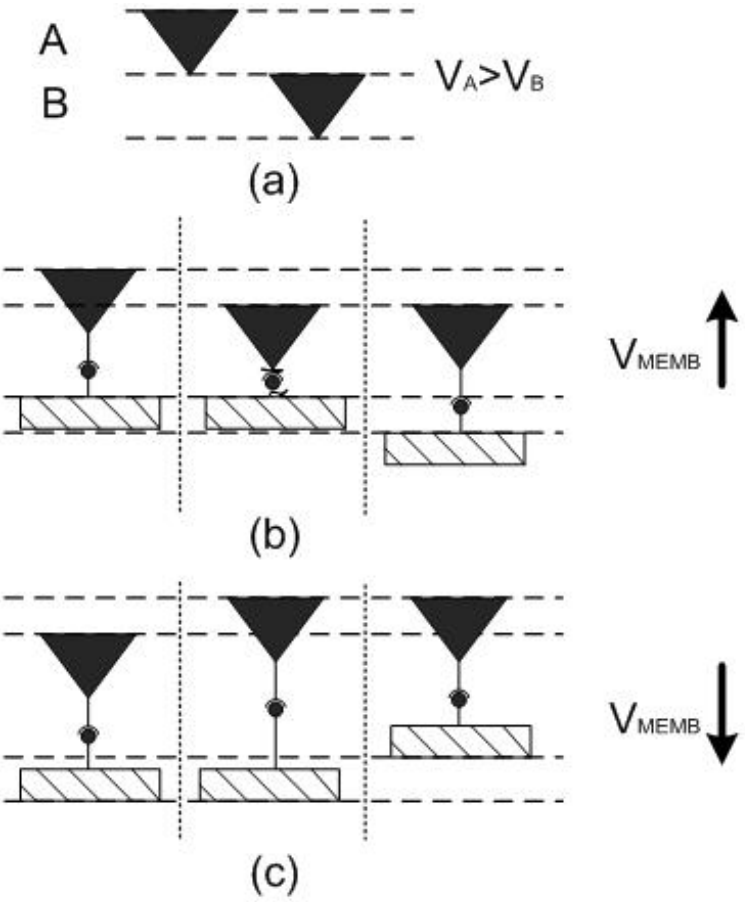

Figure 39: Illustrations to demonstrate how the feedback system operates. Piezo is stationary and only the cantilever tip is considered (described by the triangle shape). The membrane is shown by the rectangular surface.

data is stored in a *.xls* file for future processing.

CHAPTER IV

RESULTS AND DISCUSSION

To prove the control system is operating correctly, it is important to test it in biological experiments, which will demonstrate its capability in obtaining significant data.

4.1 Feasibility Demonstration

As was discussed previously, a modified version of the control system was used to show its feasibility with loading rate experiments. For simplicity reasons, the experiment was first preformed by controlling the piezo actuator instead of the membrane. Figure 40 show the result of this test run.

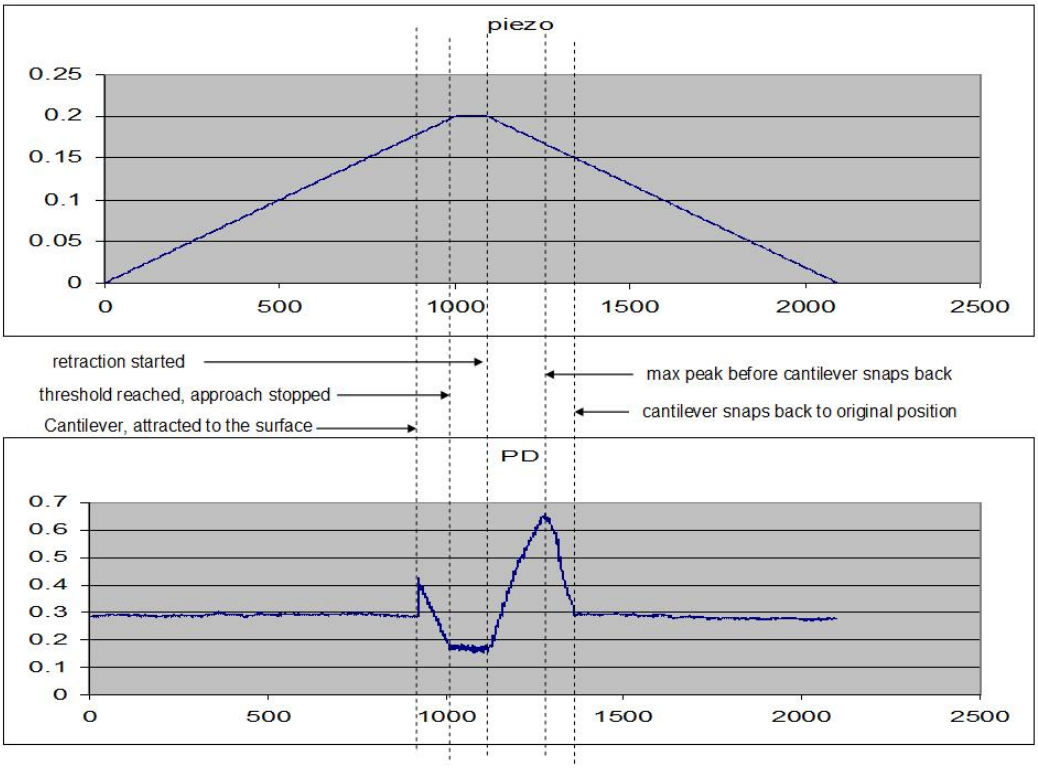

Figure 40: Loading rate experiments using the piezo actuator and performing the displacement readout from the membranes backside.

The top graph shows the displacement signal to the piezo actuator while the lower graph shows the cantilever displacement as a function of time. The figure shows that the cantilever displacement follows the piezo displacement. The system was

then connected to the membrane actuator to show that the conversion tool described earlier would produce the desired membrane displacement signal. Figure 41 shows the results of this run.

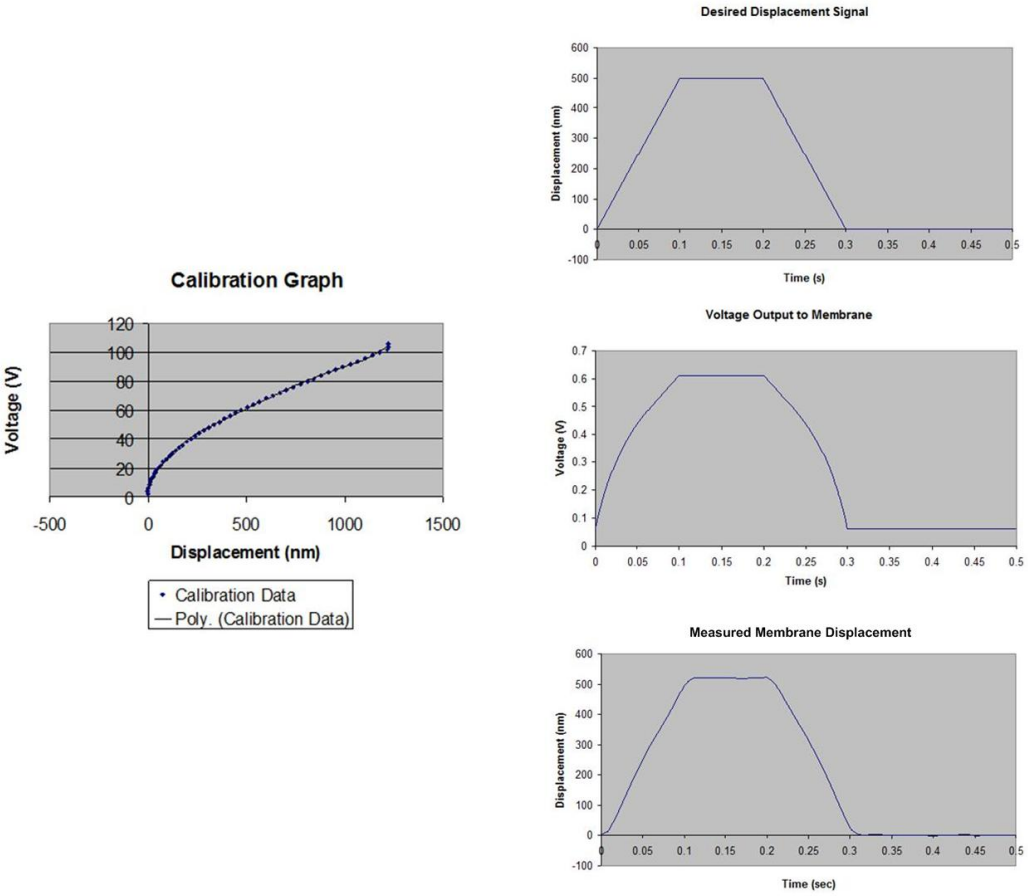

Figure 41: Loading rate experiments using the membrane actuator.

As seen in the figure, the control system used the membrane voltage-displacement calibration curve (shown to the left side of the figure) to create a conversion function which is denoted by the polynomial fit of the calibration graph. This conversion function was then used to convert the desired displacement signal (top graph in Figure 41) into the required membrane voltage (second graph from the top). The final membrane displacement is shown at the bottom graph of the figure. The membrane displacement shows that as the displacement values approached zero there was a

discrepancy from the desired signal. This error arises due to mismatch in the lower value between the polynomial fit used to describe the data and the actual data. To avoid this problem the user can specify displacement values which will start from a higher value and will have a better fit with the calibration data. Overall the results show that by modifying the program, loading rate experiment can be easily run. This thesis mainly focuses on the force-clamp experiments, and therefore this control scheme was only demonstrated as a proof of principle.

To test the basic performance of the force clamp control system, the cantilever was brought into direct contact with the membrane using the AFM piezo system. This process was described earlier in this thesis. A non-zero force was obtained by pressing on the membrane with the cantilever. To simulate force disturbances in the system, the height of the z-piezo drive was changed manually by the user. The voltage to the membrane was captured along with the photodiode output to analyze the regulatory behavior of the feedback loop system. Figure 42 shows the membrane actuation signal as applied by the DAQ card along with the force reading captured by the photodiode.

The data obtained from the experiment was further processed and filtered using Matlab R2008a (Simulink, Version 7.6). The results are shown in Figure 43.

The blue line in the figure shows the filtered force signal outputted by the photodiode. This curve shows the force between the cantilever and membrane as a function of time, where the cantilever is in direct contact with the membrane. The force value was initially set to 9200 pN by manually moving the z-piezo using the Dimension AFM system. The green line shows the voltage on the membrane supplied by the DAQ card as a function of time. The sudden peaks in the force curve are the result of intentional force disturbances which are obtained by changing the z-piezo position (this procedure was described earlier in this chapter). As seen by the membrane voltage curve, the voltage on the membrane followed the force change experienced by the

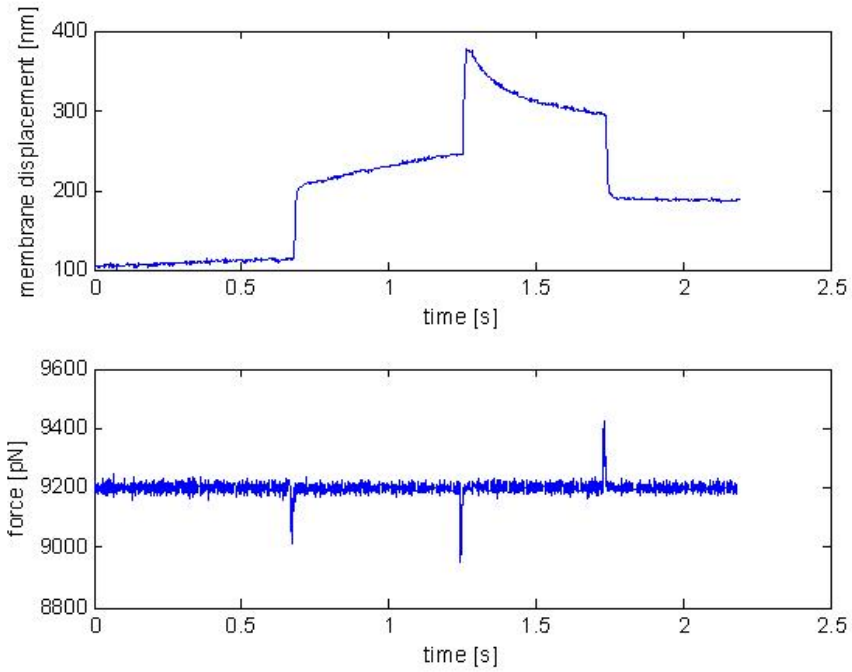

Figure 42: Demonstration of the feedback loop system using a cantilever in direct contact with a membrane.The force was set to 9200 pN.

cantilever. The force disturbances were immediately compensated to bring the force back to its original value of 9200 pN. The z-piezo was tested with different values to simulate force disturbances in both z directions. It is easily shown in the figure, that the membrane voltage is compensated proportionally with respect to the size of the disturbance.

Figure 44 shows the result of a similar experiment in which an additional rupture force was being simulated. When the force disturbance exceeded a certain value specified by the user, the program assumed a rupture event has occurred and the feedback loop was exited.

The initial force value was set to 450 pN. Due to the large voltage change required for compensation in the final disturbance (after $\sim$45 seconds) a rupture event was identified. In this case the feedback loop was exited automatically which shows that it was operating correctly. The force in the system can also be updated during the

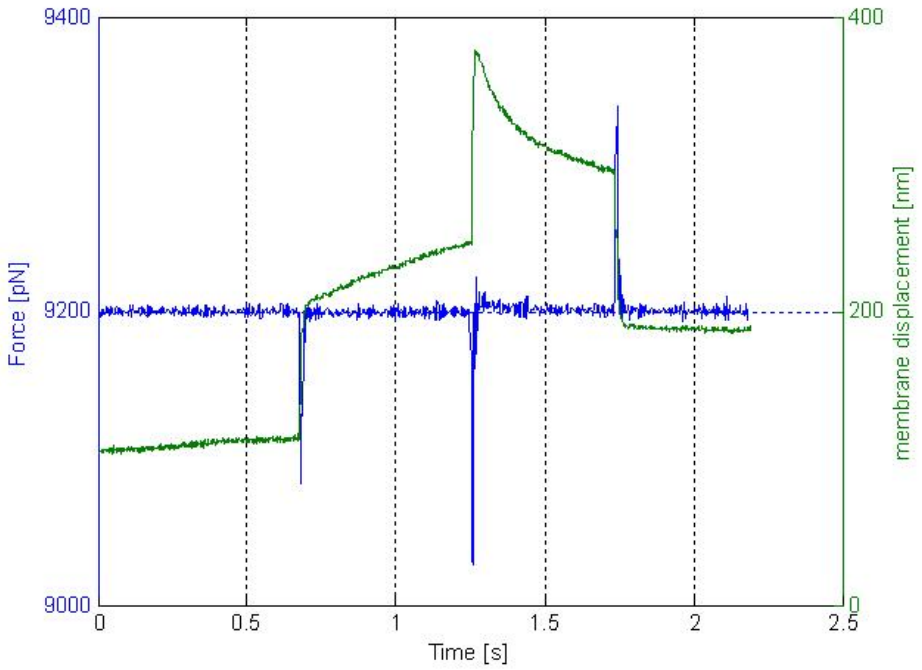

Figure 43: Filtered data of the force between the cantilever and membrane as a function of time.

process of the experiment, as seen by Figure 45.

In this experiment the force was initially set to 100 pN, and then increased to 200 pN, 250 pN, and 350 pN. To increase the force on the biomolecule the program increased the voltage on the membrane, as seen by the green curve in the figure.

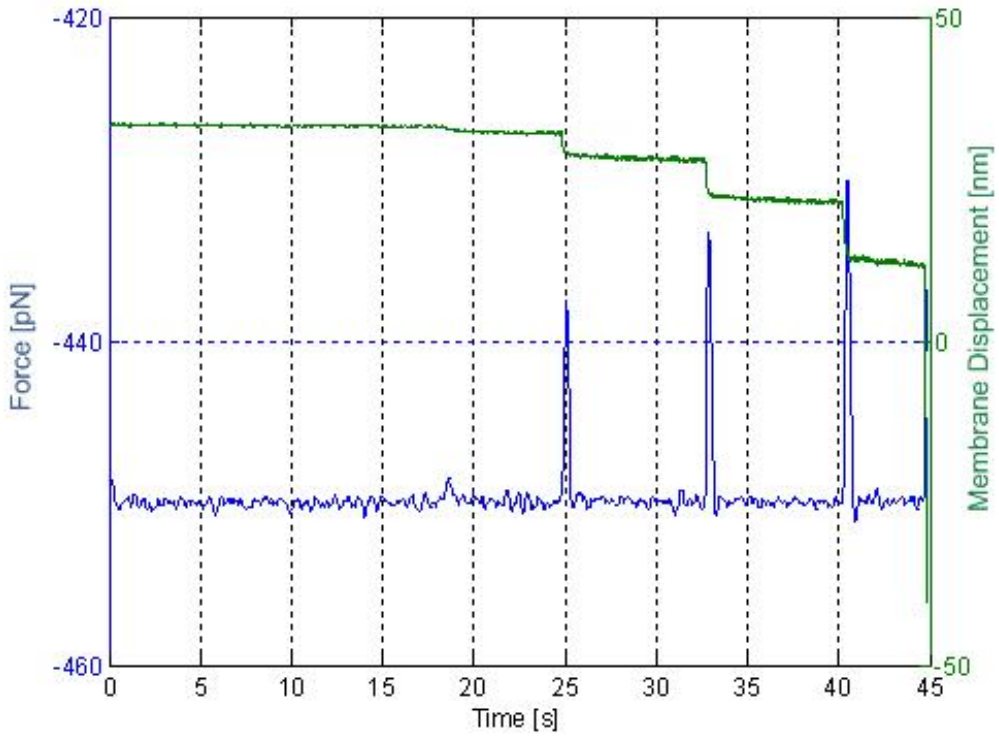

Figure 44: Simulation of a rupture force when testing the feedback loop.

4.2 Biological Experiments

The feasibility of this system with biomolecules was tested using human and anti-human IgG. After the incubation period which was described in section 3.1, the cantilever was brought into contact with the membrane using the z-piezo. After the biomolecules were bonded together a specified force value was entered into the system and the membrane was pulled down until the desired force was reached. Figure 46 shows the data taken from the force clamp experiment.

The top graph in the figure shows the force as a function of time. The value for the force was set to 130 pN. Because the initial value of the force was smaller than the specified force, an initial drop in force is shown. The graph maintains a constant value until a rupture event occurred at around 0.9 seconds for a force of 100 pN ($SET\ I$), and 0.37 seconds for a force of 80 pN ($SET\ II$). While the force was shown to

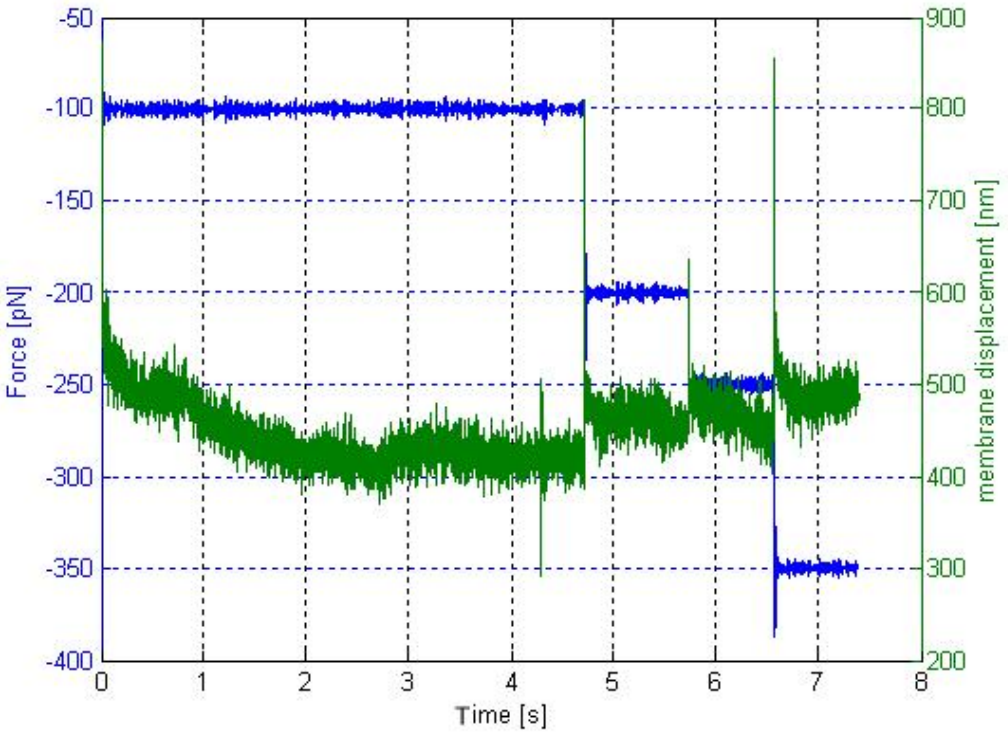

Figure 45: Force value changing, by the user, during the experiment.

be maintained at a constant value, the membrane displacement graph (bottom graph of both *SET I* and *SET II* in Figure 46) shows fluctuations in the displacements which indicates that the force was fully compensated.

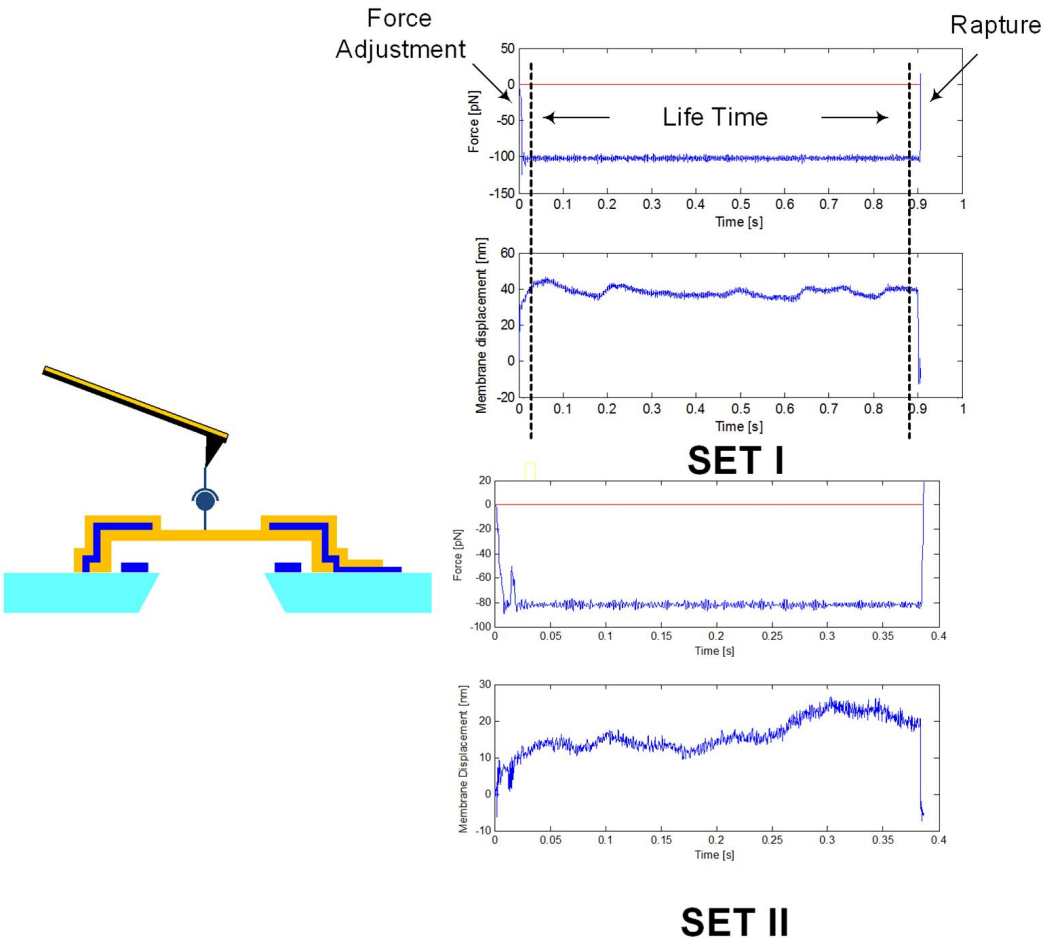

Figure 46: Force clamp experiments using the control system described previously in this thesis.

4.3 RF Drive for Membrane Actuation

While DC voltage biases tend to break down the membrane insulation, AC voltage signals having amplitudes higher than 75 V and frequencies of up to 600 kHz did not result in short circuit failures. Electrolysis did not occur because the average voltage on the membrane in the AC mode was approximately zero (during the experiment the value was found to be -1.43 μV). As long as the average voltage was kept under the decomposition voltage of 1.28 V, electrolysis did not occur. The carrier frequency needs to be larger than the membrane's frequency response if the signal is to be modulated completely. Figure 47 shows a modulated signal and its corresponding

membrane displacement as captured by the AFM photodiode.

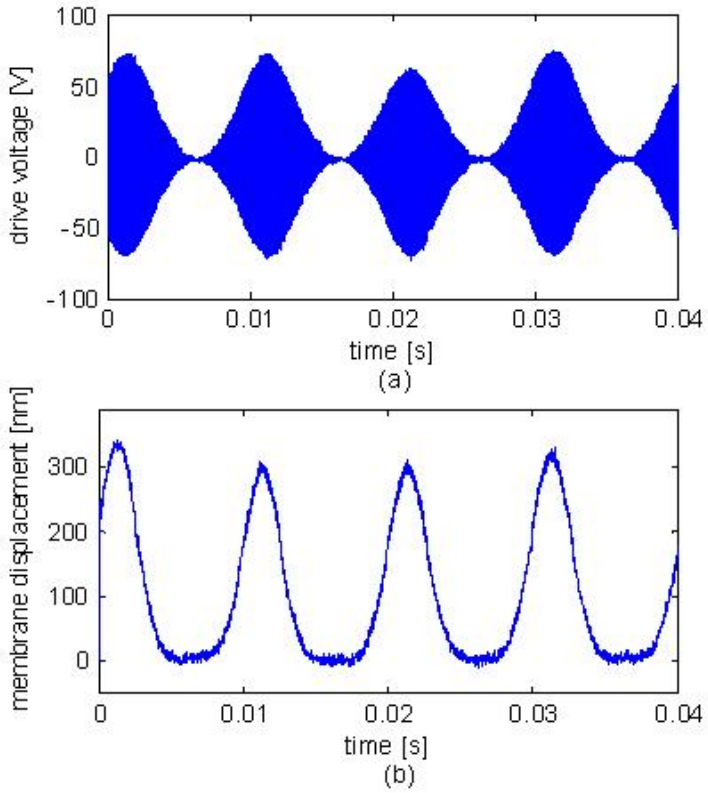

Figure 47: Modulated signal. Carrier frequency at 600 kHz.

Figure 47 shows a fully modulated signal, which demonstrates that this method is applicable for these experiments and can be used in order to avoid electrolysis. The carrier frequency of this signal was 600 kHz, which is considerable higher than the frequency response of the membrane, used in the experiment, which at most has 100 kHz frequency response (as mentioned earlier). Using Figure 23, the membrane displacement is shown to have full correlation with the membrane voltage signal.

An important issue in analyzing the experimental data was to detect the limiting factor for force detection in this system. Therefore, the noise spectrum of all the components in the system were measured. To noise spectrum was measured using a spectrum analyzer (SR760, Stanford Research Systems), which was connected to the photodiode output of the AFM system. Figure 48 shows the results of the noise

spectrum analysis.

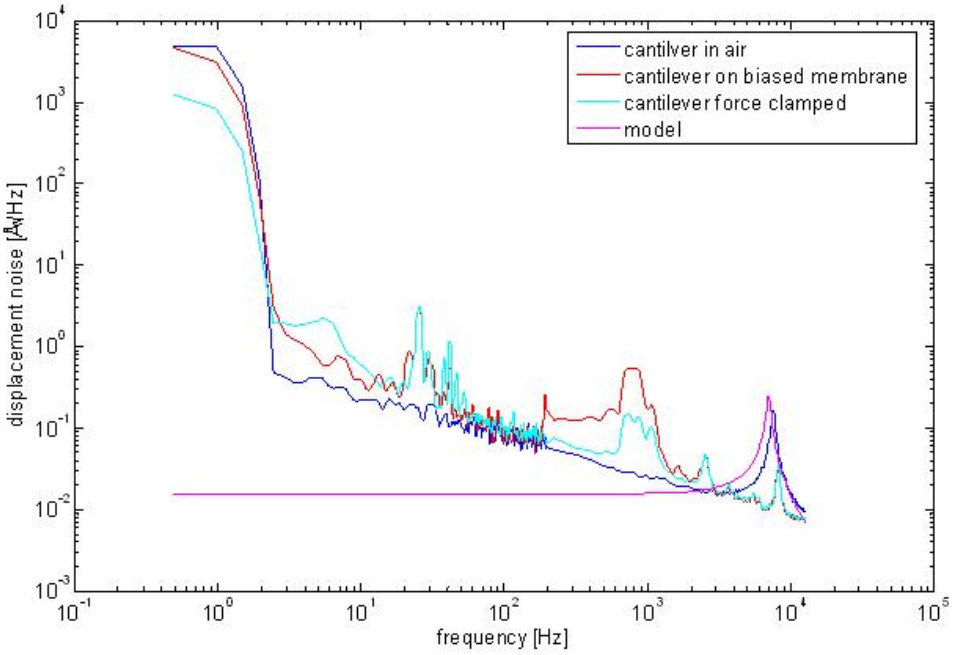

Figure 48: Noise spectrum of the cantilever at different positions.

The cantilever frequency response model is shown in pink. The discrepancy between the flat portion of the model with the one from the cantilever in air (blue line), is due to the viscoelastic damping [27], which was not considered in the model. As seen from the experimental results the cantilever noise in air is fairly similar to the noise spectrum received during a force clamp experiment, and during the time the cantilever was engaged on a biased membrane. Figure 49 shows a further analysis of the system noise spectrum while using the RF modulation scheme.

The figure shows the noise spectrum of the cantilever in air, the cantilever engaged to the membrane while the membrane is biased using the RF amplifier, the cantilever in contact with the substrate, and the cantilever engaged to the membrane while the membrane is not biased (although connected to the RF amplifier). This graph shows that the noise spectrum of the cantilever in air (blue line) is similar to the other noise spectrum from the other cantilever positions.

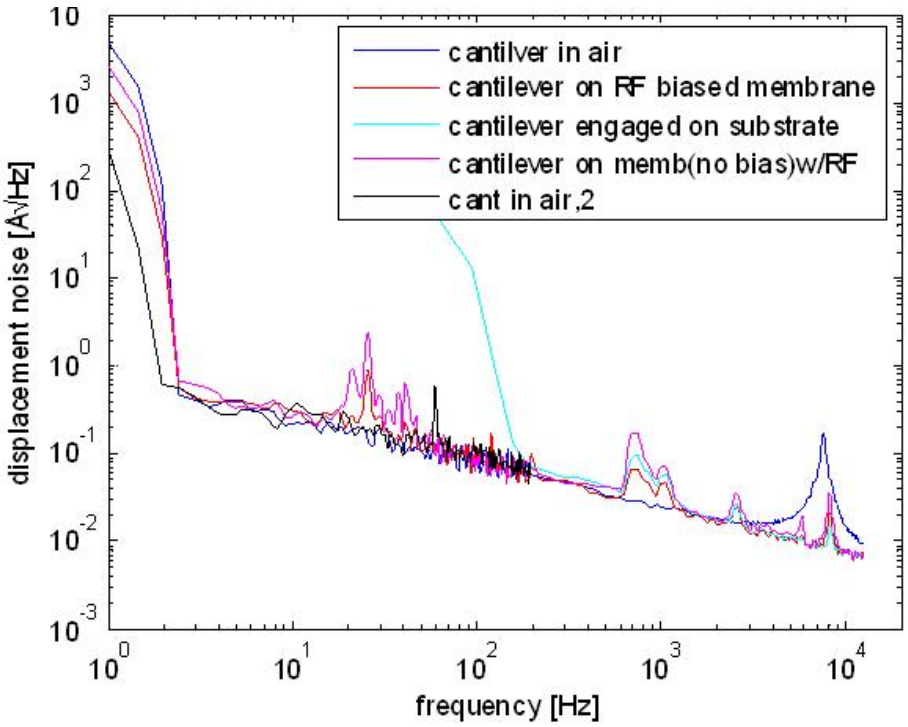

Figure 49: Noise spectrum analysis of the cantilever when AC modulation was used.

The peaks at around 1000 Hz and 2500 Hz, also identified in Figure 48, are not shown when the cantilever is in air but are noticeable when the cantilever is engaged to the substrate. This means that the noise at these frequencies is probably the result of mechanical noise from the setup table.

These noise spectrum results show that the components added to the system did not introduce any additional noise and also recognizes the cantilever as the slowest device among those involved in the feedback loop of this system.

CHAPTER V

CONCLUSION

This thesis presented the development of a control system for a membrane actuator, which was used in force spectroscopy experiments. The system used both an open loop system, which was used to demonstrate the feasibility of this system in loading rate experiments, and a closed loop system, which was used for force-clamp experiments. Both control schemes relayed on the AFM optical detection system to record the forces on the biomolecule, using the cantilever as the force sensor.

In the loading rate control system, the program created a conversion tool between the membrane's voltage and displacement by fitting a polynomial on the membrane's calibration curve. This conversion tool was later on used to linearize the membrane motion which is inherently non-linear. In the force-clamp control system, the feedback loop monitored for any changes to the force, and compensated for them by changing the voltage on the membrane actuator. It was shown that the complexity introduced by this control system did not affect the noise level in the system and identified the cantilever as the limiting factor.

Actuation system such as the bulk piezo actuator, known as the "picocube", demonstrated a frequency response of 10 kHz [26]. Another system which uses photothermal cantilever actuator [35], showed to have an even larger actuation bandwidth of 12.5 kHz which was mainly limited by the frequency response of their actuator. This system on the other hand, demonstrated an actuation bandwidth of up to 100 kHz. This difference can have a significant improvement in the response time.

Furthermore this system can be implemented on any AFM system without changing the mechanical design of the AFM system. In order to do so, the user only needs to place the membrane devices on the AFM stage under the piezo head, and run the control system, which was implemented using LabVIEW. This characteristic makes this control scheme more convenient when compared with other systems which do not hold this capability.

Backside readout capabilities have been demonstrated before with similar membrane designs [38]. By implementing this capability in this setup it is possible to improve the feedback bandwidth of the force sensor considerable to reach the actuator limit of 100 kHz.

Improvement of the system can be achieved by developing a parallel readout system. This can significantly increase the throughput of the measurements which is highly desirable in biological experiments.

APPENDIX A

FORCE CLAMP PROGRAM

A.1 Interface

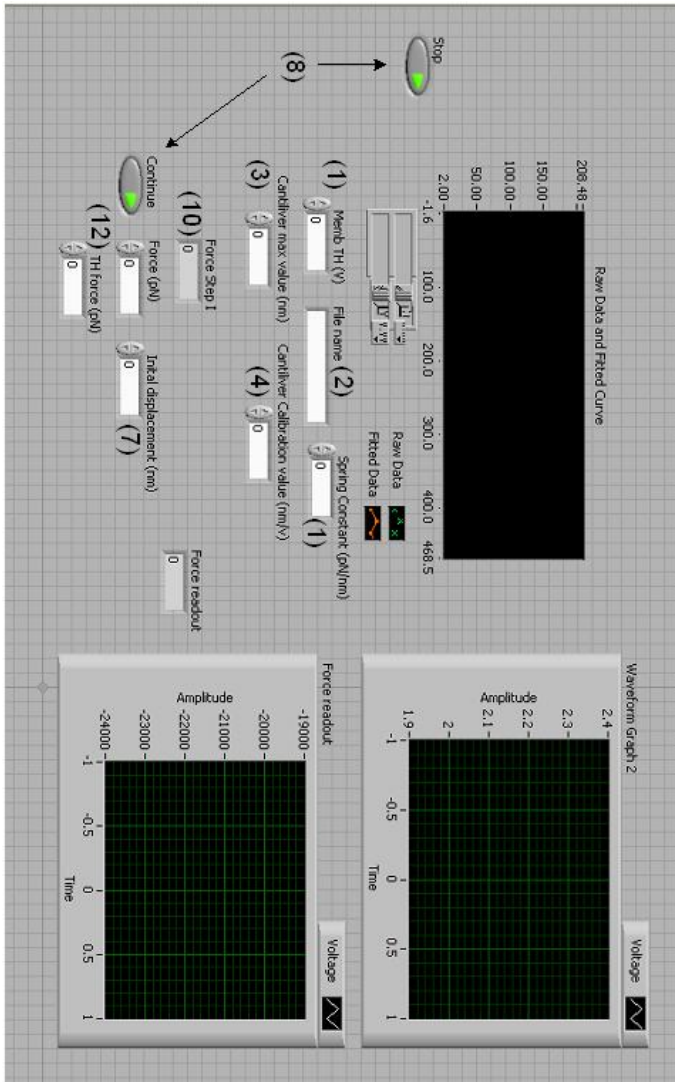

A.2 Instructions

1. Specify the membrane threshold voltage in the $MembTH$ control (maximum voltage on the membrane) and the cantilever spring in Spring Constant.

2. Enter the desired file name for the results. The files will be stored in the folder $c:\backslash krishna\backslash$.

   Two files will be created:

   (a) "name you picked"_mem_voltage_"today's date".xls - stores the membrane deflection data (displacement (nm) vs. time (s)).

   (b) "name you picked"_Force_"today's date".xls - stores the results obtained from the experiment (force (pN) vs. time (s)).

   (c) "name you picked"_mem_cali_"today's date".xls - stores the membrane calibration data (voltage (V) vs. displacment (nm)). This information is also displayed in Raw Data and Fitted Curve.

3. Specify the Cantilever maximum displacement value. This is done in order to stop the experiment in the case were the membrane collapses before the specified threshold value is reached.

4. Input the Cantilever Calibration value obtained from the dimension system (also known as the cantilever sensitivity).

5. Connect the following connections on the DAQ:

   (a) Connect $ai0$ to the photodiode output (input the cantilever displacement in volts).

   (b) Connect $ao0$ to the piezo amplifier (output the membrane displacement in volts).

6. Bring the cantilever into contact with the membrane using the dimension 3100 system.

7. Specify the Initial displacement. The membrane will be initially deflected to allow force control in both directions.

8. Make sure both the press buttons in the program are set to off.

9. Run the program.

10. The program will give the current force value in the $Force\ StepI$, in pN.

11. By using the "pull up" and "pull down" functions on the dimension system the user will manually set the force on the biomolecule to a value close to the desired force.

12. The user will then specify the force in Force and the threshold force in $THforce$.

13. Press the continue button and keep it pressed until the force as a function of time at the Force readout graph will be displayed. The instantaneous force will be displayed at the Force readout indicator, in pN.

Note:

1. While running the program you can change the force value.

2. You can stop the program from running at any time by pressing the stop button.

APPENDIX B

PULLING PROGRAM

B.1 Interface

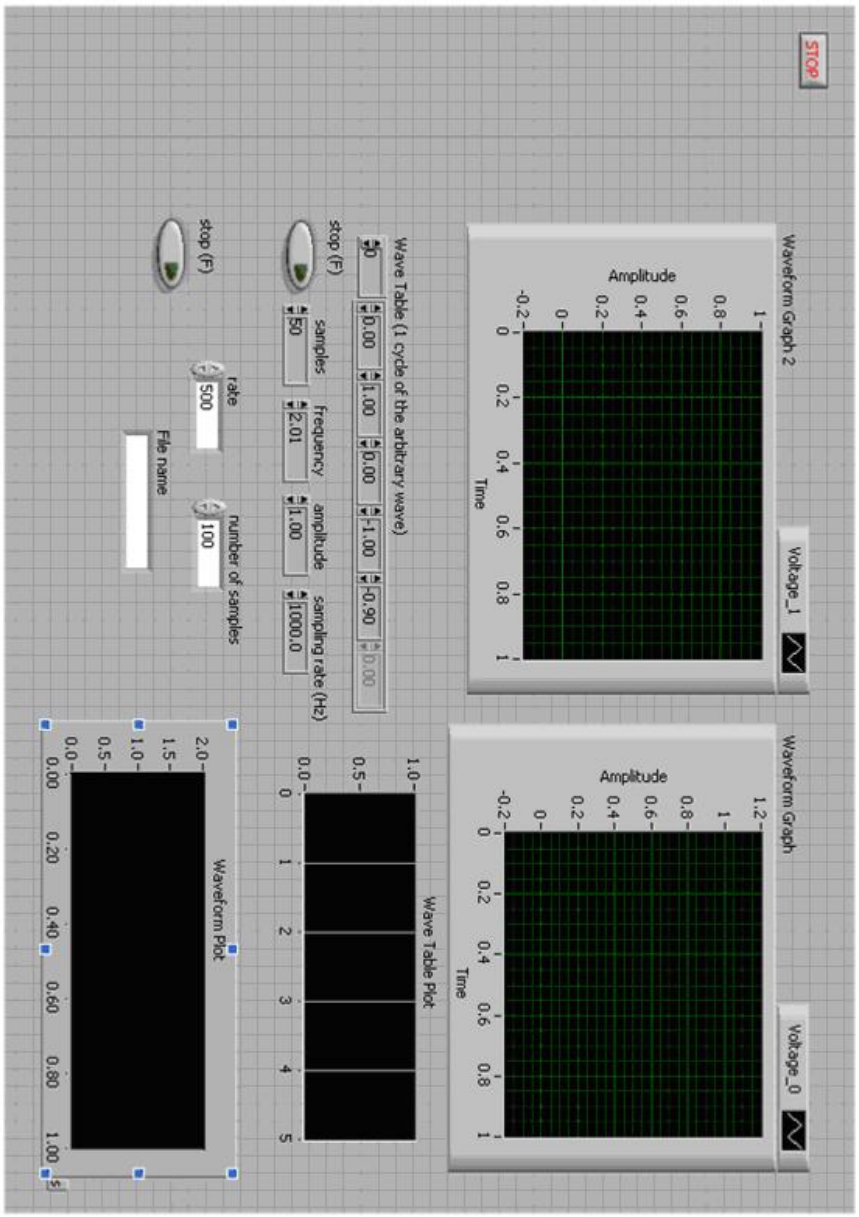

B.2 Instructions

1. Create the desired signal using the *Displacement Table*. You can specify six different values, in *nm*, and the program will connect them via a straight line. This portion of the signal is shown in the *Signal Table Plot*. The portion of the signal will be repeated continuously to create the desired signal which is shown in the *Signal Plot graph*. The actual signal to the membrane, in volts, is shown in *Output to Mem*.

2. Input the amount of samples in this portion of the signal, amplitude (this value will be multiplied by the value of each point on the signal), sampling rate and cycles for the signal. By controlling these values you are able to control the pulling speeds.

3. Input the readout rate in *rate*, and number of samples in *number of samples*.

4. Enter the desired file name for the results. The data will be stored at $c : \backslash krishna \backslash$ "name you picked"_output_"today's date".xls which will store the Photodiode displacement (nm) and the piezo displacement (nm) as a function of time (V).

5. Input the Cantilever Calibration value obtained from the dimension system (also known as the cantilever sensitivity).

6. Connect the following connections on the DAQ:

   (a) Connect $ai0$ to the photodiode output (input the cantilever displacement in volts).

   (b) Connect $ao0$ to the piezo amplifier (output the piezo displacement in volts).

7. Bring the cantilever into contact with the membrane using the dimension 3100 system.

8. Run the program.

Note:

1. While running the program you can change the force value.

2. You can stop the program from running at any time by pressing the stop button.

APPENDIX C

CALIBRATION PROGRAM

C.1 Interface

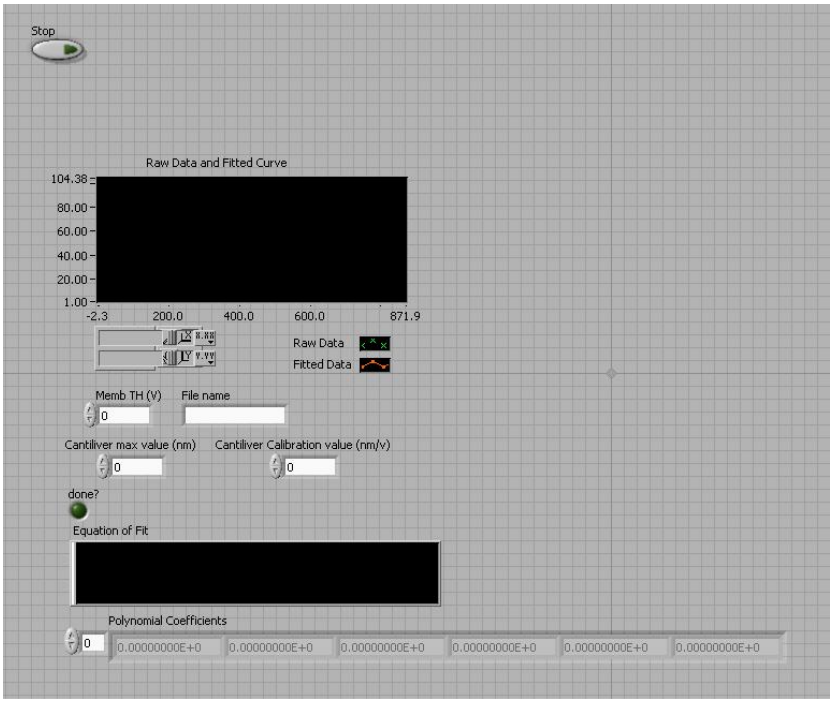

C.2 Instructions

1. Specify the membrane threshold voltage in the $MembTH$ control (maximum voltage on the membrane).

2. Enter the desired file name for the results. The files will be stored in the folder $c:\backslash krishna\backslash$.

   The file that will be created: "name you picked"_mem_voltage_"today's date".xls - stores the membrane calibration data (voltage (V) vs. displacment (nm)). This information is also displayed in $RawData$ and $FittedCurve$.

3. Specify the Cantilever maximum displacement value. This is done in order to stop the experiment in the case were the membrane collapses before the specified threshold value is reached.

4. Input the cantilever calibration value obtained from the dimension system (also known as the cantilever sensitivity).

5. Connect the following connections on the DAQ:

   (a) Connect $ai0$ to the photodiode output (input the cantilever displacement in volts).

   (b) Connect $ao0$ to the membrane (output the membrane displacement in volts).

6. Bring the cantilever into contact with the membrane using the dimension 3100 system.

7. Run the program.

APPENDIX D

NI PCI-6229 CARD [17]

Analog Input	
Number of channels	
NI 6224/6229	16 differential or 32 single ended
ADC resolution	16 bits
INL	Refer to the AI Absolute Accuracy Table
Sampling Rate	
Maximum	250 kS/s single channel 250 kS/s multi-channel (aggregate)
Minimum	No minimum
Timing Accuracy	50 ppm of sample rate
Timing Resolution	50 ns
Input coupling	DC
Input range	$\pm 10\ V$, $\pm 5\ V$, $\pm 1\ V$, $\pm\ 0.2\ V$
Maximum working voltage for analog inputs (signal + common mode)	$\pm 11\ V$ of AI GND
CMRR (DC to 60 Hz)	92 dB
Crosstalk (at 100 kHz)	
Adjacent channels	-75 dB
Non-adjacent channels	-90 dB
Input FIFO size	4,095 samples
Scan list memory	4,095 entries

Analog Output	
Number of channels	
NI 6229	4
DAC resolution Maximum update rate	16 bit
1 channels	833 kS/s
2 channels	740 kS/s per channel
3 channels	656 kS/s per channel
4 channels	625 kS/s per channel
Timing Accuracy	50 ppm of sample rate
Timing Resolution	50 ns
Output range	$\pm$ 10 V
Output coupling	DC
Output FIFO size	8,191 samples shared among channels used

APPENDIX E

NI BNC-2110 FRONT PANEL [16]

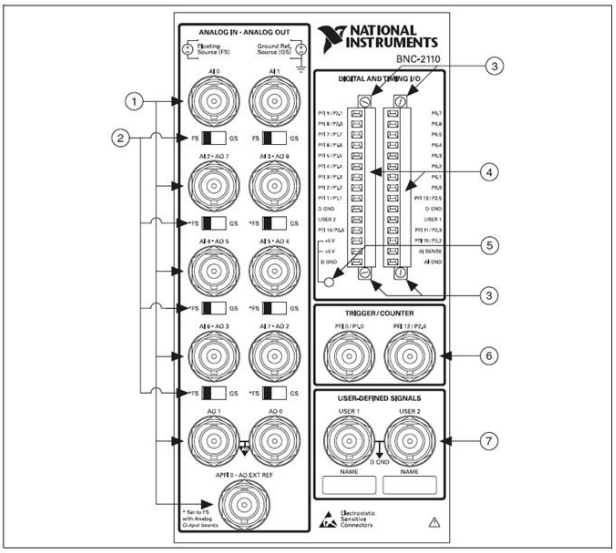

1	Analog Input/Analog Output BNC Connectors	5	Power Indicator Light
2	FS/GS Switches	6	Trigger/Counter BNC Connectors
3	Terminal Block Retaining Screws	7	User-Defined Signals BNC Connectors
4	Digital and Timing I/O Spring Terminal Blocks		

APPENDIX F

E-507 HVPZT AMPLIFIER MODULES (COURTESY OF PHYSIK INSTRUMENTE)

F.1 Frequency Response

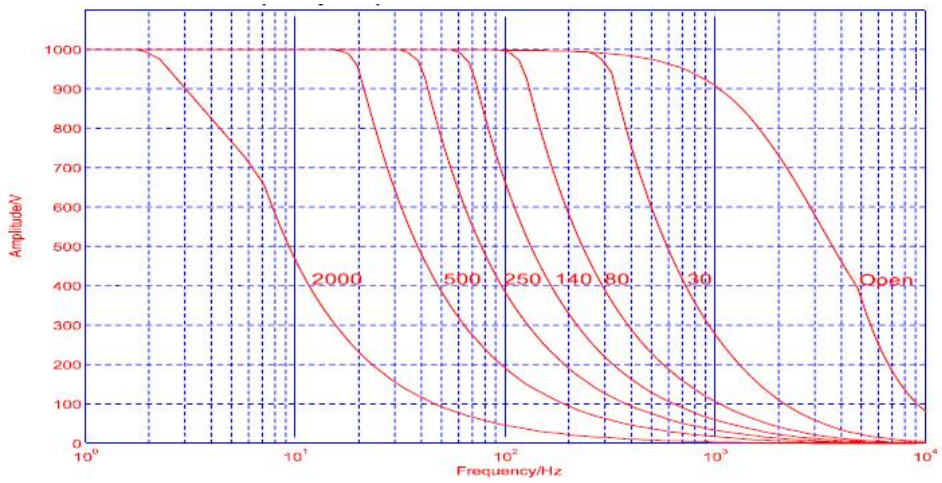

Frequency response with various PZT loads. Values shown are capacitance in nF measured in actual PZT.

REFERENCES

[1] Ando, T., Uchihashi, T., Kodera, N., Yamamoto, D., Miyagi, A., Taniguchi, M., and Yamashita, H., "High-speed AFM and nano-visualization of biomolecular processes," *Pflügers Archiv European Journal of Physiology*, vol. 456, no. 1, pp. 211–225, 2008.

[2] Ashkin, A. and Dziedzic, J., "Optical trapping and manipulation of viruses and bacteria," *Science*, vol. 235, no. 4795, pp. 1517–1520, 1987.

[3] Baumgartner, W., Hinterdorfer, P., Ness, W., Raab, A., Vestweber, D., Schindler, H., and Drenckhahn, D., "Cadherin interaction probed by atomic force microscopy," 2000.

[4] Beyder, A., Spagnoli, C., and Sachs, F., "Reducing probe dependent drift in atomic force microscope with symmetrically supported torsion levers," *Review of Scientific Instruments*, vol. 77, p. 056105, 2006.

[5] Di Giovanni, M., *Flat and corrugated diaphragm design handbook*. CRC Press, 1982.

[6] Dimension, T., "3100 Series Scanning Probe Microscope Instruction Manual. 1998," *Digital Instruments: Santa Barabara, CA*.

[7] Evans, E., "P ROBING THE R ELATION B ETWEEN F ORCE-L IFETIME-AND C HEMISTRY IN S INGLE M OLECULAR B ONDS," *Annual Review of Biophysics and Biomolecular Structure*, vol. 30, no. 1, pp. 105–128, 2001.

[8] Fernandez, J. and Li, H., "Force-clamp spectroscopy monitors the folding trajectory of a single protein," 2004.

[9] Friedsam, C., Wehle, A., Kuhner, F., and Gaub, H., "Dynamic single-molecule force spectroscopy: bond rupture analysis

with variable spacer length," *Journal of Physics Condensed Matter*, vol. 15, no. 18, pp. 1709–1724, 2003.

[10] Fritz, J., Katopodis, A., Kolbinger, F., and Anselmetti, D., "Force-mediated kinetics of single P-selectin/ligand complexes observed by atomic force microscopy," *Proceedings of the National Academy of Sciences of the United States of America*, vol. 95, no. 21, p. 12283, 1998.

[11] Griffin, C., *Inorganic quantitative analysis*. Read Books, 2007.

[12] Grover, W., Skelley, A., Liu, C., Lagally, E., and Mathies, R., "Monolithic membrane valves and diaphragm pumps for practical large-scale integration into glass microfluidic devices," *Sensors & Actuators: B. Chemical*, vol. 89, no. 3, pp. 315–323, 2003.

[13] Hall, N., Bicen, B., Jeelani, M., Lee, W., Qureshi, S., Degertekin, F., and Okandan, M., "Micromachined microphones with diffraction-based optical displacement detection," *The Journal of the Acoustical Society of America*, vol. 118, p. 3000, 2005.

[14] Hinterdorfer, P., Baumgartner, W., Gruber, H., Schilcher, K., and Schindler, H., "Detection and localization of individual antibody-antigen recognition events by atomic force microscopy," 1996.

[15] Hung, E. and Senturia, S., "Extending the travel range of analog-tuned electrostatic actuators," *Microelectromechanical Systems, Journal of*, vol. 8, no. 4, pp. 497–505, 1999.

[16] Instruments, N., "Installation Guide BNC-2110," *National Instruments: Austin, TX*, 2007.

[17] Instruments, N., "Low-Cost M series Multifunction Data Acquisition - 16 Bit, 250 kS/s, up to 80 Analog Inputs," *National In-struments: Austin, TX*, 2008.

[18] Kishino, A. and Yanagida, T., "Force measurements by micromanipulation of a single actin filament by glass needles," 1988.

[19] Knight, J. and Degertekin, F., "Capacitive micromachined ultrasonic transducers for forward looking intravascular imaging arrays," in *2002 IEEE Ultrasonics Symposium, 2002. Proceedings*, vol. 2, 2002.

[20] Levy, R. and Maaloum, M., "Measuring the spring constant of atomic force microscope cantilevers: thermal fluctuations and other methods," *Nanotechnology*, vol. 13, no. 1, pp. 33–37, 2002.

[21] Lou, J., Yago, T., Klopocki, A., Mehta, P., Chen, W., Zarnitsyna, V., Bovin, N., Zhu, C., and McEver, R., "Flow-enhanced adhesion regulated by a selectin interdomain hinge," *Journal of Cell Biology*, vol. 174, no. 7, p. 1107, 2006.

[22] Marszalek, P., Lu, H., Li, H., Carrion-Vazquez, M., Oberhauser, A., Schulten, K., and Fernandez, J., "Mechanical unfolding intermediates in titin modules," *Nature*, vol. 402, no. 6757, pp. 100–103, 1999.

[23] Merkel, R., Nassoy, P., Leung, A., Ritchie, K., and Evans, E., "Energy landscapes of receptor–ligand bonds explored with dynamic force spectroscopy," *Nature*, vol. 397, no. 6714, pp. 50–53, 1999.

[24] Oberhauser, A., Hansma, P., Carrion-Vazquez, M., and Fernandez, J., "Stepwise unfolding of titin under force-clamp atomic force microscopy," *Proceedings of the National Academy of Sciences*, vol. 98, no. 2, p. 468, 2001.

[25] Onaran, A., Balantekin, M., Lee, W., Hughes, W., Buchine, B., Guldiken, R., Parlak, Z., Quate, C., and Degertekin, F., "A new atomic force microscope probe with force sensing integrated readout and active tip," *Review of Scientific Instruments*, vol. 77, p. 023501, 2006.

[26] One, B., "The PicoCube–The Worlds Smallest Piezo Scanner,"

[27] Paolino, P. and Bellon, L., "Frequency dependence of viscous and viscoelastic dissipation in coated micro-cantilevers from noise measurement," 2009.

[28] Rief, M., Gautel, M., Oesterhelt, F., Fernandez, J., and Gaub, H., "Reversible unfolding of individual titin immunoglobulin domains by AFM," *Science*, vol. 276, no. 5315, p. 1109, 1997.

[29] Sarangapani, K. K., Torun, H., Finkler, O., Zhu, C., and Degertekin, L., "A Membrane-based AFM Actuation Approach for High Speed Dynamic Force Spectros-copic Experiments," 2009.

[30] Schlierf, M., Li, H., and Fernandez, J., "The unfolding kinetics of ubiquitin captured with single-molecule force-clamp techniques," *Proceedings of the National Academy of Sciences*, vol. 101, no. 19, pp. 7299–7304, 2004.

[31] Senturia, S., *Microsystem design*. Kluwer Academic Publishers.

[32] Simson, D., Ziemann, F., Strigl, M., and Merkel, R., "Micropipet-based pico force transducer: in depth analysis and experimental verification," *Biophysical journal*, vol. 74, no. 4, pp. 2080–2088, 1998.

[33] Smith, S., Finzi, L., and Bustamante, C., "Direct mechanical measurements of the elasticity of single DNA molecules by using magnetic beads," *Science*, vol. 258, no. 5085, pp. 1122–1126, 1992.

[34] Spagnoli, C., Beyder, A., Besch, S., and Sachs, F., "Drift-free atomic force microscopy measurements of cell height and mechanical properties," *Review of Scientific Instruments*, vol. 78, p. 036111, 2007.

[35] Stahl, S., Puchner, E., and Gaub, H., "Photothermal cantilever actuation for fast single-molecule force spectroscopy," *Review of Scientific Instruments*, vol. 80, p. 073702, 2009.

[36] Strunz, T., Oroszlan, K., Schafer, R., and Guntherodt, H., "Dynamic force spectroscopy of single DNA molecules," 1999.

[37] Torun, H., Finkler, O., and Degertekin, F., "Athermalization in atomic force microscope based force spectroscopy using matched microstructure coupling," *Review of Scientific Instruments*, vol. 80, p. 076103, 2009.

[38] Torun, H., Sutanto, J., Sarangapani, K., Joseph, P., Degertekin, F., and Zhu, C., "A micromachined membrane-based active probe for biomolecular mechanics measurement," *Nanotechnology*, vol. 18, no. 16, pp. 165303–165500, 2007.

[39] Veijola, T., Kuisma, H., Lahdenper
"a, J., and Ryh
"anen, T., "Equivalent-circuit model of the squeezed gas film in a silicon accelerometer," *Sensors & Actuators: A. Physical*, vol. 48, no. 3, pp. 239–248, 1995.

[40] Viani, M., Schäffer, T., Chand, A., Rief, M., Gaub, H., and Hansma, P., "Small cantilevers for force spectroscopy of single molecules," *Journal of Applied Physics*, vol. 86, p. 2258, 1999.

[41] Wenzler, L., Moyes, G., and Beebe Jr, T., "Improvements to atomic force microscopy cantilevers for increased stability," *Review of Scientific Instruments*, vol. 67, p. 4191, 1996.